Cellular/Molecular

ICAM-1 Deletion Using CRISPR/Cas9 Protects the Brain from Traumatic Brain Injury-Induced Inflammatory Leukocyte Adhesion and Transmigration Cascades by Attenuating the Paxillin/FAK-Dependent Rho GTPase Pathway

Bibhuti Ballav Saikia,[1]* Saurav Bhowmick,[1]* Anitha Malat,[1] M. R. Preetha Rani,[1] Almas Thaha,[1] and P. M. Abdul-Muneer[1,2]

[1]Laboratory of CNS injury and Molecular Therapy, JFK Neuroscience Institute, Hackensack Meridian Health JFK University Medical Center, Edison, New Jersey 08820 and [2]Department of Neurology, Hackensack Meridian School of Medicine, Nutley, New Jersey 07110

Intercellular adhesion molecule-1 (ICAM-1) is identified as an initiator of neuroinflammatory responses that lead to neurodegeneration and cognitive and sensory–motor deficits in several pathophysiological conditions including traumatic brain injury (TBI). However, the underlying mechanisms of ICAM-1–mediated leukocyte adhesion and transmigration and its link with neuroinflammation and functional deficits following TBI remain elusive. Here, we hypothesize that blocking of ICAM-1 attenuates the transmigration of leukocytes to the brain and promotes functional recovery after TBI. The experimental TBI was induced in vivo by fluid percussion injury (25 psi) in male and female wild-type and *ICAM-1*$^{-/-}$ mice and in vitro by stretch injury (3 psi) in human brain microvascular endothelial cells (hBMVECs). We treated hBMVECs and animals with ICAM-1 CRISPR/Cas9 and conducted several biochemical analyses and demonstrated that CRISPR/Cas9-mediated ICAM-1 deletion mitigates blood–brain barrier (BBB) damage and leukocyte transmigration to the brain by attenuating the paxillin/focal adhesion kinase (FAK)-dependent Rho GTPase pathway. For analyzing functional outcomes, we used a cohort of behavioral tests that included sensorimotor functions, psychological stress analyses, and spatial memory and learning following TBI. In conclusion, this study could establish the significance of deletion or blocking of ICAM-1 in transforming into a novel preventive approach against the pathophysiology of TBI.

Key words: **CRISPR/Cas9; functional recovery; intercellular adhesion molecule-1; leukocytes; paxillin–FAK; Rho GTPase; transmigration; traumatic brain injury**

Significance Statement

Intercellular adhesion molecule-1 (ICAM-1) has a significant role in the regulation of vascular permeability and the transmigration of leukocytes to the brain. The regulatory role of ICAM-1 in the transmigration of leukocytes to the brain and its downstream pathways and its link with functional deficits following traumatic brain injury (TBI) are not clear. In this study, using an in vitro stretch injury in human brain microvascular endothelial cells and an animal model of fluid percussion injury, we demonstrated that the deletion of ICAM-1 using the method of CRISPR/Cas9 (clustered regularly interspaced short palindromic repeats/CRISPR-associated protein 9) protects the brain from TBI-induced inflammatory leukocyte adhesion and transmigration cascades by attenuating the paxillin/FAK-dependent Rho GTPase pathway.

Received Sept. 15, 2023; revised Jan. 9, 2024; accepted Jan. 27, 2024.

Author contributions: P.M.A.-M. designed research; B.B.S., S.B., A.M., M.R.P.R., and A.T. performed research; B.B.S., S.B., and P.M.A.-M. analyzed data; P.M.A.-M. wrote the paper.

This work was supported by the New Jersey Commission on Brain Injury Research grant number CBIR19PIL010, the National Institutes of Health (NIH) grant number 1R21AA030625, and the Neuroscience Institute at JFK University Medical Center, Edison, New Jersey, to P.M.A.-M.

*B.B.S. and S.B. contributed equally to this work.

The authors declare no competing financial interests.

Correspondence should be addressed to P. M. Abdul-Muneer at Mohammed.Muneer@hmhn.org.

https://doi.org/10.1523/JNEUROSCI.1742-23.2024

Introduction

Leukocyte adhesion and transmigration cascades are the major hallmarks of traumatic brain injury (TBI)-induced neuroinflammation that leads to brain tissue damage and impairments of sensory/motor and cognitive functions (Schwarzmaier et al., 2013; Bhowmick et al., 2021). Although several factors are involved in the mechanisms of the transmigration of leukocytes to the brain, recently, we have demonstrated that intercellular adhesion molecule 1 (ICAM-1) is one of the key regulators of

the transmigration of leukocytes after TBI (Bhowmick et al., 2021). ICAM-1, a recognized family of adhesion molecules, is encoded by the *ICAM-1* gene primarily found in endothelial cells, epithelial cells, fibroblast, keratinocytes, and some immune cells (Bui et al., 2020). Recently, we reported that ICAM-1 has a significant role in neuroinflammation, neurodegeneration, and impairing of cognitive and sensory–motor functions after TBI (Bhowmick et al., 2021). Evidence from clinical studies suggests that antisense oligonucleotide drug shows potential in reducing the production of ICAM-1 and subsequent reduction in inflammatory responses in other diseases like Crohn's disease and multiple myeloma (Di Fusco et al., 2019; Xu et al., 2019). In addition, administration of anti-ICAM-1 antibody showed improvement in motor function after an experimental TBI in rats (Knoblach and Faden, 2002) and recovery from ICAM-1 mediated cerebrovascular endothelium damage in response to injury (Lutton et al., 2017). However, in this study, deleting ICAM-1 using the modern molecular CRISPR/Cas9 tool, we analyzed the potential role in the transmigration of leukocytes to the brain by attenuating paxillin/focal adhesion kinase (FAK)-dependent Rho GTPase pathway and demonstrated the protection of the brain from further neuroinflammation and functional impairments.

Focal adhesions (FAs) are clusters of receptors that play a potent role in leukocyte adhesion and transmigration (Parsons et al., 2012). The two FA proteins paxillin and FAK regulate many cellular processes of transmigration of immune cells (Burridge et al., 1992; Schaller, 2001), and the regulation of transmigration signaling is achieved by the phosphorylation of paxillin and FAK (Cuvelier et al., 2005). Luscinskas et al. evidenced that the silencing of both paxillin and FAK impaired neutrophil migration; however, the neutrophil adhesion was not affected (Luscinskas, 2012). Moreover, phosphorylated paxillin regulates the binding of ICAM-1 to its receptor leukocyte function-associated antigen-1 (LFA-1; Romanova and Mushinski, 2011). However, the role of paxillin and FAK in the ICAM-1–mediated transmigration of leukocytes is not well studied. Rho GTPases family (e.g., RhoA, Rac1, Cdc42) has a role in controlling a variety of cellular processes that include cell morphogenesis, proliferation, migration, and survival (Hodge and Ridley, 2016). One of the prominent members of the GTPase family, RhoA, is involved in many neurodegenerative diseases (Schmidt et al., 2022). Interestingly the previous study also suggested that a major function of paxillin is to regulate Rho family GTPases in *Drosophila* (Chen et al., 2005). Previous work demonstrated that TBI causes profound activation of RhoA signaling and hence blocking RhoA and/or ROCK signaling was discovered to be a promising strategy to prevent TBI-related cell death and neuronal damage (Mulherkar and Tolias, 2020). We recently demonstrated the significant role of ICAM-1 in neuroinflammation and neurodegeneration through the LFA-1/Mac-1 pathway that leads to sensorimotor dysfunction and psychological stress (Bhowmick et al., 2021). However, a clear role of ICAM-1 in regulating the transmigration of leukocytes via the paxillin/FAK-Rho GTPase-dependent pathway is not yet studied in TBI.

Here, we hypothesized that phosphorylation of paxillin and FAK by the induction of ICAM-1 is regulated by the Rho GTPase pathway and the deletion of ICAM-1 by CRISPR/Cas9 will protect the brain from the blood–brain barrier (BBB) damage and transmigration of leukocytes by attenuating paxillin/FAK-dependent Rho GTPase pathway. We employed CRISPR/Cas9 technology to delete ICAM-1 and demonstrated that the deletion of ICAM-1 impairs the mechanism of leukocyte transmigration through the disruption of the paxillin–FAK signaling pathway. In conclusion, this study could pave the way to establish a novel therapeutic approach against the pathophysiology of TBI through the deletion or blocking of ICAM-1.

Materials and Methods

Cell culture

Human brain microvascular endothelial cells (hBMVECs) were cultured in Dulbecco's modified Eagle's medium/F12 media supplemented with 10% heat-inactivated fetal bovine serum (FBS; Thermo Fisher Scientific), 1% penicillin, and streptomycin (Thermo Fisher Scientific), 1% amphotericin, endothelial cell growth supplement (50 mg/ml; BD Biosciences), heparin (100 mg/ml; Sigma-Aldrich). hBMVECs were plated on rat tail collagen-coated (0.1 mg/ml) 6-well Bioflex culture plates (Flexcell International) at a density of 250,000 cells/well and grown until confluence. The cells were fed by changing the medium every 2 d, and hBMVECs were grown to confluence before use.

ICAM-1 CRISPR/Cas9 and siRNA treatments

To remove ICAM-1, the CRISPR/Cas9 genome editing approach using the AAV vector was applied in hBMVECs. The transduction was carried out by adding the vector particles to the cells 30 min prior to cell injury in a half volume of serum-free medium for 1 h and followed by the addition of another half volume with 20% FBS. The hBMVECs were treated with the CRISPR AAV (1.1×10^7 GC/ml) as per the manufacture's instruction. The cell lysates and culture supernatant were collected for further analysis. The cytotoxicity of ICAM-1 CRISPR/Cas9 AAV treatment was evaluated by MTT [3-(4,5-dimethylthiazol-2-yl)-2,5-diphenyltetrazolium bromide] assay. The average cell death in ICAM-1 CRISPR/Cas9, control CRISPR/Cas9, and untreated cells were 3.72, 3.46, and 3.45%, respectively, and these values are not significant to each other.

ICAM-1 siRNA transfection was carried out as per the manufacturer's instruction (Santa Cruz Biotechnology). The 60–80% confluent hBMVECs were washed once with plain media and incubated with 1 ml siRNA transfection medium containing 2–8 µl siRNA duplex (0.25–1 µg siRNA) at 37°C in a CO_2 incubator for 6 h. Without removing the transfection mixture, then 1 ml of normal growth medium containing two times the normal serum and antibiotic concentration (2× normal growth medium) was added and the cells were incubated for an additional 18–24 h. Then the fresh 1× normal growth medium was replaced, and the stretch injury was conducted. The scrambled control siRNA was used to compare the effect of ICAM-1 siRNA. Twenty-four hours after a stretch injury, cells were fixed for immunostaining, or proteins and mRNA were extracted for Western blotting, and qPCR, respectively.

In vitro stretch injury

The cultured hBMVECs were subjected to stretch injury using a biaxial in vitro cell injury device, "cell injury controller II" (Custom Design and Fabrication) with a pressure of 3.0 psi (Patel et al., 2017; Abdul-Muneer et al., 2018; Bhowmick et al., 2019a; Bhowmick et al., 2021) with a pulse duration of 50 ms. Twenty-four hours poststretch injury, cells were fixed for immunostaining, proteins were extracted for Western blotting, and RNA was isolated for qRT-PCR experiments.

Animals, fluid percussion injury, and CRISPR treatments

Male and female C57/BL6 mice wild-type (WT) and *ICAM-1*$^{-/-}$ mice (9 weeks old, 20–25 g; Jackson Laboratory) were used for this study. Animals were maintained in sterile cages under pathogen-free conditions in accordance with institutional ethical guidelines for the care of laboratory animals, the National Institutes of Health, and the Seton Hall University Institutional Animal Care and Use Committee. We used a diurnal 12 h light cycle in our animal facility, and we carried out surgeries for fluid percussion injury (FPI) during the light cycle. Standard surgical methods for lateral FPI were performed in 10-week-old male mice (Taconic Biosciences; (Bhowmick et al., 2018b, 2019b). Rectal temperatures were continuously monitored and maintained within normal ranges during surgical preparation by a feedback temperature controller pad (model TC-1000; CWE). Before the injury, mice were anesthetized with 5% isoflurane until the foot-pinch reflex stopped. The animal was connected to a digitally controlled FPI system-FP302 (Amscien

Instruments), and the injury was applied through the needle hub positioned 3.0 mm posterior from and 2.5 mm lateral from the bregma at 25 psi (8–10 animals/group) with a pressure rise time of 8 ms. Similarly, control mice received the same anesthesia and surgery as the injury group and connected to the dc-FPI without the injury. Eight to ten animals per group were used and are sufficient to get statistically significant results as per our previously reported studies and power analysis (Faul et al., 2007; Bhowmick et al., 2018b; Abdul-Muneer et al., 2022).

One hour after the injury, the CRISPR/Cas9 AAV was injected at a concentration of 2×10^8 genome copies (GC) per milliliter stereotactically (Kim et al., 2014) through a stepper-motorized microsyringe (Stoelting) at a rate of 1 µl/5 min. CRISPR/Cas9 AAV was injected into four sites below the injury area in the cortex; that is, posterior 2.0 mm, lateral 2.5 mm, depth 1.0 mm; posterior 3.0 mm, lateral 3.5 mm, depth 2.0 mm; posterior 4.0 mm, lateral 2.5 mm, depth 1.5 mm; and posterior 3.0 mm, lateral 2.0 mm, depth 1.5 mm from bregma. The results were compared with control CRISPR AAV injected TBI or uninjured animals. After 2 weeks, animals were anesthetized with a ketamine/xylazine mixture and transcardially perfused with 1× PBS and then 4% paraformaldehyde. Autopsied brain tissues were kept frozen until analyzing the mechanisms of pathophysiology by immunohistochemical staining analysis (tissue-embedded OCT for staining), qPCR, Western blotting, immunoprecipitation, and ELISA as per our well-established protocols (Abdul Muneer et al., 2012; Abdul-Muneer et al., 2013; Bhowmick et al., 2021). In Figure 1*A*, the schematic representation of the whole animal procedure is given.

CRISPR validation

ICAM-1 CRISPR/Cas9 genome editing efficiency in hBMVEC culture was determined using the Genomic Cleavage detection method. In this method, DNA from ICAM-1 CRISPR-edited hBMVECs was used as a template in PCR reactions and amplified with ICAM-1 primers specific to the targeted region. In our experiment, the PCR product of the ICAM-1 gene-targeted region is expected to have a product size of 565 bp size. In cleavage assay, the PCR products are denatured and rehybridized, which produces mismatches in the double-stranded DNA, and the detection enzyme recognizes and cleaves the mismatches, producing two fragments. In our cleavage experiment, the target product was cleaved at 199 and 366 bp. Agarose gel electrophoresis showed three bands—an uncleaved band at 565 bp and two cleaved bands at 199 and 366 bp. This demonstrates the efficiency of ICAM-1-targeted CRISPR editing. We included control samples supplied by the manufacturer to perform control PCR reaction, and this served as a control for denaturing, reannealing, and enzyme digestion steps. This control template has a size of 750 bp after PCR amplification and 500 and 250 bp after the cleavage assay. In agarose gel analysis, three bands with 750, 500, and 250 bp were visualized. Next, we used a gel imaging system to take images and gel analysis software (AlphaImager Software); a microfluidic electrophoresis bioanalyzer was used to determine the relative proportion of DNA contained in each band. The cleavage efficiency was calculated from the band densities of the parental band and cleaved bands using the formula given below. The efficiency of ICAM-1 gene knock-out in endothelial cells was determined, and our data show 25% of DNA was genetically modified in CRISPR-edited samples.

The cleavage efficiency is calculated by the following equation:

$$\text{Cleavage Efficiency} = 1-[(1-\text{fraction cleaved})^{1}/_{2}].$$

$$\text{Fraction Cleaved} = \text{sum of cleaved band intensities} / (\text{sum of the cleaved and parental band intensities}).$$

Immunostaining

Immunofluorescence. We carried out immunofluorescence staining in both cultured endothelial cells (on silicone membrane) and 10-µm-thick coronal brain sections as previously described (Bhowmick et al., 2018a; 2019a). Cells and tissue sections were washed with 1× PBS and fixed using 4% paraformaldehyde for 20 min at 25°C. After washing with 1× PBS, pH 7.4, for 5 min, the cells and cryostat sections were blocked in 3% normal goat serum containing 0.1% Triton X-100 (5% heat-inactivated BSA, PBS at pH 7.4) for 1 h at room temperature and then incubated with the appropriate primary antibodies (3.0 µg/ml; Table 1) overnight at 4°C. Cells were then washed three times in 1× PBS at room temperature for 15 min and incubated with secondary antibodies [Alexa Fluor 488 or 594 conjugated with anti-mouse or anti-rabbit immunoglobulin G (IgG) according to the primary antibodies; 1:500 dilution or 4 µg/ml] for 1 h and mounted with 5–10 µl immunomount containing DAPI (Invitrogen) on a slide. Semiquantitative analysis of the protein of interest was done as previously described (Bhowmick et al., 2021), and images were captured using a laser confocal microscope (Stellaris 5, Leica) and LAS X Stellaris (Leica) software in three channels, DAPI (cell nuclei), Alexa Fluor-488 (green color emission), and Alexa Fluor-594 (red color emission). The imaging was

Table 1. Details of the antibodies used for this study

Antibodies	Dilution	Catalog number	RRID	Vendor
Anti-β-actin	WB: 1:1,000	MA575739	AB_2545348	Thermo Fisher Scientific
Anti-ICAM-1	WB: 1:1,000; IHC: 1:250	MA5407	AB_223596	Thermo Fisher Scientific
Anti-Mac-1	WB: 1:1,000; IHC: 1:250	nb11089474	AB_1216361	Novus Biologicals
Anti-LFA-1	WB: 1:1,000; IHC: 1:250	ab186873	Not available	Abcam
Anti-paxillin	WB: 1:1,000	ab32084	AB_779033	Abcam
Anti-p-Rac1	WB: 1:1,000	ab203884	Not available	Abcam
Anti-p-Src	WB: 1:1,000	ab185617	AB_2924399	Abcam
Anti-RhoA	WB: 1:1,000	ab187027	AB_2827434	Abcam
Anti-occludin	WB: 1:1,000	ab31721	AB_881773	Abcam
Anti-claudin-5	WB: 1:1,000	ab15106	AB_301652	Abcam
Anti-N-cadherin	WB: 1:1,000	ab18203	AB_444317	Abcam
Anti-CD68	WB: 1:1,000; IHC: 1:250	ab955	AB_307338	Abcam
Anti-vWF	IHC: 1: 250	Ab11713	AB_298501	Abcam
Anti-JAM-a	WB: 1:1,000	Sc53623	AB_784134	Santa Cruz Biotechnology
Anti-connexin-43	WB: 1:1,000	3512S	AB_2294590	Cell Signaling Technology
Anti-FAK	WB: 1:1,000	3285S	AB_2269034	Cell Signaling Technology
Anti-p-FAK	WB: 1:1,000	3283S	AB_2173659	Cell Signaling Technology
Anti-Src	WB: 1:1,000	2108S	AB_331137	Cell Signaling Technology
Anti-Cdc42	WB: 1:1,000	4651S	AB_10612265	Cell Signaling Technology
Anti-p-paxillin	WB: 1:1,000	2541S	AB_2174466	Cell Signaling Technology
Anti-Rac1	WB: 1:1,000	GTX100761	AB_10618495	GeneTex

IHC, immunohistochemistry; WB, Western blotting.

performed by a researcher who was blinded to the experimental conditions, and the area of image capture was randomized. The intensity of immunostaining was analyzed by ImageJ (NIH) software (Bankhead, 2014). See more details in the experimental design and statistical analysis section.

HRP-substrate immunohistochemistry. HRP-substrate immunohistochemistry was performed in 10-µm-thick paraformaldehyde-fixed coronal brain tissue sections on a glass slide. After washing the tissue sections in 1× PBS, the tissue sections were incubated with 0.3% H_2O_2 in 1× PBS and 0.3% Triton X-100 for 20 min at RT. Then, after washing three times in 1× PBS, the tissue was blocked in 4% normal goat serum in phosphate buffer containing 0.3% Triton X-100 for 1 h at room temperature. Then the tissue sections were incubated with primary antibodies (Table 1) overnight at 4°C. Using 1× PBS, the primary antibody was rinsed off three times, and the tissues were incubated with 1:200 HRP goat secondary antibody in PBS containing 0.3% Triton X-100 for 1 h at RT followed by three washes with 1× PBS. Then the tissue sections were incubated with the peroxidase substrate reagent (SK-4600; VectorLabs) mixed with 0.02% H_2O_2 for 5–10 min to observe the color changes under a dissecting microscope. Then after three times washing with 1× PBS, tissue slides were mounted with histomount and glass coverslips for microscopy analyses.

Western blotting

Protein was extracted from the cultured cells and 50 mg brain tissue (from the injury area), and cells or tissue were lysed using Cell Lytic MT Cell Lysis Buffer (Thermo Scientific) containing a mixture of Mini Protease Inhibitor Cocktail Tablets (Sigma-Aldrich). The quantity of the extracted protein was measured by bicinchoninic acid (BCA) assay (Thermo Fisher Scientific). Immunoblots were performed by resolving the protein (15 µg) in 4–15% gradient SDS-PAGE gel (Bio-Rad), and the blots were transferred onto a nitrocellulose membrane and blocked with (5%) skim milk for 1 h at room temperature. After removing the blocking reagent, the primary antibody (Table 1) was added to the membranes and incubated overnight at 4°C. After washing three times for 15 min each, the membranes were incubated for 1 h at room temperature with horseradish peroxidase-conjugated secondary antibodies (1:5,000; Fisher Scientific). The membrane was rinsed three times with TBS-Tween for 15 min at RT. Protein bands were detected using chemiluminescence Western blot detection reagents (Advansta) and scanned with an imaging system GE Healthcare ImageQuant LAS 4000. The optical density was quantified as arbitrary densitometry intensity units using the ImageJ software package (NIH). The protein of interest was normalized and quantified using β-actin as a loading control.

Co-immunoprecipitation

The interaction between ICAM-1 and its receptors LFA-1 and Mac-1 was analyzed by co-immunoprecipitation (co-IP) using Pierce Classic Magnetic IP/Co-IP kit (catalog #88804; Bhowmick et al., 2021). Approximately 50 mg of brain tissue from WT and *ICAM-1*$^{-/-}$ mice with and without FPI was collected, and tissues were lysed with 250 ml of cell lysis buffer followed by centrifugation, and the supernatant was then transferred to a new tube for determining the protein concentration. In this experiment, Pierce Protein A/G Magnetic Beads were used for IP according to the manufacturer's instructions. For each sample, 500 µg of total protein extract was subjected to an IP assay. The protein samples were incubated with 10 µg of anti-ICAM-1 antibody at 4°C overnight. Following the formation of the immune complex, A/G Magnetic Beads were added and incubated for 1 h. Further, the IP complex was washed, and the samples were suspended in 100 µl of sample buffer. Finally, 20 µl of samples was subjected to Western blotting using ICAM-1, LFA-1, and Mac-1 antibodies.

Monocyte adhesion assay in vitro

The adhesion of immune cells to the hBMVEC monolayer was quantitatively analyzed in vitro as previously reported (Schmitz et al., 2013; Sha et al., 2015; Li et al., 2016; K. Xu et al., 2022). For this, hBMVECs were cultured on rat tail collagen-coated (0.1 mg/ml) 6-well Bioflex culture plates at a density of 250,000 cells/well and grown until confluence, and after the formation of the tight monolayer (approximately 2–3 d), the cells were treated with ICAM-1 CRISPR/Cas9, control CRISPR/Cas9, ICAM-1 siRNA, or control siRNA 30 min prior to the injury as per the manufacturer's protocol (see above, ICAM-1 CRISPR/Cas9 and siRNA treatments and In vitro stretch injury sections). Twenty-four hours after the injury, Calcein-AM–labeled (a green fluorescence cell tracker; 2 µM, Invitrogen) primary human monocytes were introduced into the endothelial monolayers (1×10^6 monocytes/well). Cells were then allowed to adhere for 2 h at 37°C in a tissue culture incubator. Nonadherent cells were then washed with 1× PBS and removed, and cells were lysed subsequently. The relative fluorescence intensity of the adhered cells was detected by a fluorescence-based assay using the Tecan GENios fluorescence plate reader, and spectrofluorometric quantification was performed at 492 nm (excitation) and 535 nm (emission) on a 96-well plate reader. The actual numbers of adhered monocytes were calculated from the internal standard curve of the labeled cells, and the data were presented as the fold difference of the untreated control.

Transmigration assay in vivo

As we previously reported (Abdul Muneer et al., 2012), the bone marrow was separated (by flushing out repeatedly using a 1 ml syringe with sterile 1× HBSS) from the femoral bones of euthanized GFP transgenic mice (strain: C57BL/6-Tg(CAG EGFP)131Osb/LeySopJ) under sterile conditions and washed in 1× PBS. The bone marrow suspension was filtered through a 40 mm cell strainer. The bone marrow filtrate was centrifuged at 2,000 rpm for 5 min at 4°C. The pellet was suspended in 1 ml of DMEM/F-12 media containing 10% FBS, penicillin, and streptomycin (100 mg/ml each, Invitrogen) and 0.001% macrophage colony-stimulating factor (MCSF; 500 µl in 500 ml media). Then the cells were dissociated by trituration (10–15 times) and counted with trypan blue using a hemocytometer. Bone marrow-derived GFP monocytes were differentiated into macrophages, and after 6 d, the differentiated macrophages were separated and suspended in 1 ml HBSS. Then the suspension was centrifuged at 2,000 rpm for 5 min at 4°C. The collected cell pellets were then dissociated by repeated trituration and counted. The GFP macrophages (2×10^6) were infused through the common carotid artery using a 30 G needle. The animals were euthanized 1 h after the cell infusion, and then the brain tissue sections were prepared and observed for GFP macrophages under the fluorescent microscope.

Blood–brain barrier permeability assay

The BBB permeability after a brain injury was measured by infusing sodium fluorescein (NaFl) and Evans Blue (EB) tracer dye mixtures (5 µM each) into the common carotid artery 24 h after the injury. Two hours later, the brains were removed, weighed, and homogenized in 600 µl 7.5% (w/v) trichloroacetic acid (TCA). The homogenized suspensions were divided into two aliquots (300 µl each). In one aliquot, 50 µl 5 N NaOH was added and neutralized. Then the NaFl was measured by fluorimetry on a GENios microplate reader (excitation 485 nm, emission 535 nm). The second aliquot was centrifuged at 10,000 rpm for 10 min at 4°C, and the supernatant was measured by absorbance spectroscopy at 620 nm for EB determination. A standard curve was constructed by serial dilutions of a standard EB/NaFl solution in 7.5% TCA.

ELISA

Using the commercial ELISA kits, the quantification of ICAM-1 (Abcam), VEGF-A (catalog #BMS-277-2), CXCL-8 (IL-8; catalog #KHC0081), IL-1β (catalog #88-7013-22), and TNF-α (catalog #88-7324-22) all from Life Technologies–Thermo Fisher Scientific were analyzed in cell culture media, tissue lysates, and blood plasma samples as per manufacturer's instructions.

Quantitative reverse transcriptase-PCR

Quantitative reverse transcriptase-PCR (qRT-PCR) was carried out to determine the mRNA expression level of ICAM-1. Total RNA from tissue samples and endothelial cells was extracted using Qiagen RNeasy Mini kit (Qiagen, catalog #74104) based on the manufacturer's protocol, and genomic contamination was removed by DNase I treatment for 20 min at 37°C. Using Qubit 2.0 (Thermo Fisher Scientific) and Agilent Bioanalyzer (Agilent Technologies), the quantity, purity, and integrity of the RNA were evaluated. Then the isolated total RNA from each sample was then

converted to cDNA using the iScript cDNA synthesis kit (Bio-Rad), and PCR amplification was performed with 25 ng of starting cDNA material mixed with gene-specific forward and reverse primers and iTaq Universal (Bio-Rad Laboratories) in a 20 µl reaction on a StepOne Real-Time System (Applied Biosystems) with standard cycling conditions (Bhowmick et al., 2021). The qPCR was performed using these primers: mouse ICAM-1 (forward, 5′-CAATTTCTCATGCCGCACAG-3′; reverse, 5′-AGCTGGAAGATCGAAAGTCCG-3′), mouse GAPDH (forward, 5′-GGTCGGTGTGAACGGATTT-3′; reverse, 5′-GTGGATGCAGGG ATGATGTT-3′). GAPDH mRNA was quantified as an endogenous control. Fold-change differences across groups were determined using the ΔΔCt method.

Behavioral study

To analyze the functional recovery after deleting ICAM-1 using CRISPR/Cas9, we carried out different behavioral measures for sensorimotor, psychological stress, and spatial memory and learning. The behavioral tests were performed on day 0 (baseline), day 2, day 7, and day 14 postinjury. All behavioral tests were conducted in the light phase of 12 h light/dark cycle, and for the light/dark test, we were cautious to not enter any light into the dark chamber. All the experimenters were blinded to the treatment groups as described previously (Bhowmick et al., 2018b, 2021). We evaluated sensory–motor deficits using the rotarod and grid walk test, the light–dark test was used to analyze anxiety, the sucrose preference test was used to analyze depression, and the Morris water maze (MWM) test was used to analyze spatial memory and learning (Vorhees and Williams, 2006; Carpenter et al., 2012; Powell et al., 2012; Ohtake et al., 2014; Bhowmick et al., 2021). Rotarod, grid walk, sucrose preference, and light–dark tests were followed exactly as we reported previously (Bhowmick et al., 2021). In MWM, the spatial acquisition period, the escape latency, and the time mouse takes to find the hidden platform were measured. In addition, probe trials for all the experimental groups were analyzed. From these probe trails, we analyzed the number of hidden platform crossings and probe time.

Experimental design and statistical analysis

Sample sizes were prospectively derived by conducting power analyses using G*Power (University of Dusseldorf, Germany), and eight to 10 animals per group were used to get statistically significant results (Faul et al., 2007; Bhowmick et al., 2018b; Abdul-Muneer et al., 2022). In hBMVECs, we repeated the experiments six times unless otherwise noted. GraphPad Prism V.9 was used for the statistical analysis of data. Significant interactions between samples/groups were achieved by ANOVA (one-way or two-way as applicable) followed by Bonferroni's post hoc tests. Data were expressed as mean ± SD, and $p < 0.05$ was considered for statistical significance. For Western blot, data were quantified using densitometry analysis using ImageJ software (Bhowmick et al., 2018a, 2019a, 2021). The immunostaining intensity or the number of positive cells was quantified using the standard method in ImageJ software (Alikunju et al., 2011; Abdul Muneer et al., 2012; Bhowmick et al., 2019a; Bhowmick et al., 2021). The analysis was performed on at least six samples for immunofluorescence staining and captured six images from a single sample (slide). The same parameters of the camera and software including the brightness of the excitation light, the detector sensitivity (gain), or the camera exposure time across the samples were used for keeping consistency during image capture. To determine the percentage of positive cells for a particular protein, we threshold the images by keeping a lower threshold level of 80 and an upper threshold level of 200. To correct for uneven illumination in fluorescence images, we kept a uniform dark background for all images. The data for the light–dark test and MWM were analyzed using the program ANY-maze v7.

Results

Expression of ICAM-1 elevates in TBI: ICAM-1 CRISPR/Cas9 modulates it

To remove ICAM-1, ICAM-1 CRISPR/Cas9 AAV (Fig. 1*B*) was injected just below the injury (FPI) area in the parietal lobe (Fig. 1*C*). Scrambled or control CRISPR/Cas9 AAV was used as control. ICAM-I CRISPR/Cas9 genome editing efficiency in human endothelial cell culture and mouse brain tissue samples was determined using a CRISPR genomic cleavage detection kit (Applied Biological Materials; catalog #G932). The PCR product of the ICAM-1 gene-targeted region is expected to have a product size of 565 bp size, and the target product of 565 bp is expected to cleave at 199 and 366 bp. In our experiment, using in vitro and in vivo approaches, we observed three bands of size 565, 366, and 199 bp in ICAM-1 CRISPR/Cas9 AAV–treated groups in both injured and uninjured samples; however, only one band of 565 bp was observed in control CRISPR/Cas9 AAV–treated groups, which demonstrates the efficiency of genomics cleavage through ICAM-1 CRISPR/Cas9 treatment (Fig. 1*D*,*E*). We included control samples supplied by the manufacturer to perform control PCR reaction, and this served as a positive control for denaturing, reannealing, and enzyme digestion steps. This control template has a size of 750 bp after PCR amplification and 500 and 250 bp after the cleavage assay. In agarose gel analysis, three bands with 750, 500, and 250 bp were visualized (Fig. 1*D*,*E*).

Next, we analyzed the expression level of ICAM-1 protein by Western blotting and immunohistochemistry. The protein expression of ICAM-1 was significantly higher in injury compared with that in uninjured controls in both stretch-injured (in vitro; 3.2-fold; $F_{(3,36)} = 335.2$; $p < 0.0001$) and FPI (in vivo; 3.25-fold; $F_{(3,36)} = 182$; $p < 0.0001$) samples (Fig. 1*F*,*G*). As expected, the expression of ICAM-1 protein was significantly reduced (to approximately one-fourth in vitro and to 0.31 in vivo) in ICAM-1 CRISPR/Cas9–treated samples compared with that in control CRISPR/Cas9–treated ones ($p < 0.0001$; Fig. 1*F*,*G*). We validated the expression of ICAM-1 protein in immunohistochemistry using an HRP-conjugated secondary antibody and its purple substrate. The expression of ICAM-1 was significantly elevated in FPI samples compared with that in uninjured controls ($F_{(5,54)} = 174.8$; $p < 0.0001$) and ICAM-1 was exclusively expressed in brain microvessels. The expression of this protein was remarkably reduced in ICAM-1 CRISPR/Cas9–treated animal samples, and ICAM-1 expression was absent in ICAM-1 KO animals (Fig. 1*H*,*I*). Similarly, when we analyzed the expression level of ICAM-1 mRNA by qRT-PCR, we observed the relative mRNA expression of ICAM-1 was upregulated in stretch-injured cells compared with that in uninjured controls in vitro (2.15-fold; $F_{(3,36)} = 83.13$; $p < 0.0001$) and in vivo (2.5-fold; $F_{(3,36)} = 216.3$; $p < 0.0001$; V). ICAM-1 CRISPR/Cas9 treatment significantly reduced the expression of mRNA compared with control CRISPR/Cas9–treated samples as we observed in the protein expression ($p < 0.0001$; Fig. 1*J*,*K*).

TBI augments the interaction of ICAM-1 with its receptors LFA-1 and Mac-1 and removal of ICAM-1 impairs the binding of ICAM-1 to its receptors

Since the binding of ICAM-1 to its receptors LFA-1 and Mac-1 is crucial in promoting adhesion and transmigration of circulating leukocytes and macrophages (Ding et al., 1999; Bhowmick et al., 2021), we next analyzed the expression of LFA-1 and Mac-1 with or without ICAM-1 CRISPR/Cas9 treatment in WT and ICAM-$1^{-/-}$ animals. Western blot analysis revealed that the expression of LFA-1 and Mac-1 was significantly increased in the FPI group compared with that in uninjured controls (LFA-1: 1.6-fold; $F_{(5,54)} = 173.2$, $p < 0.0001$; Mac-1: 2.8-fold; $F_{(5,54)} = 40.31$, $p < 0.0001$) and the treatment of ICAM-1 CRISPR/Cas9 reduced the level of LFA-1 and Mac-1 to the control level ($p < 0.0001$; Fig. 2*A*–*C*). As expected, the LFA-1 and

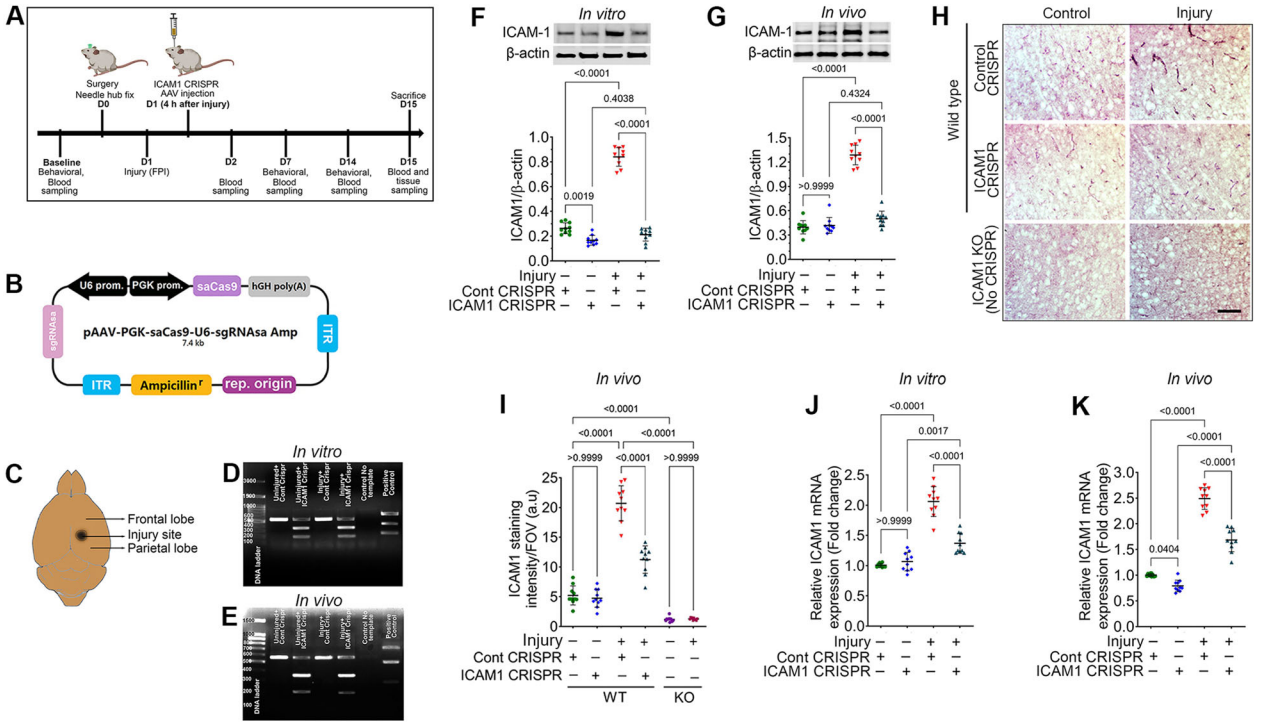

Figure 1. Activation of ICAM-1 and its receptors LFA-1 and Mac-1 after TBI in vitro and in vivo. ***A***, ***B***, Schematic representation of whole animal procedure (***A***) and ICAM-1 CRISPR/Cas9 AAV vector (***B***). ***C***, The injury (FPI) site in the mouse skull. ***D***, ***E***, PCR amplification and cleavage analysis using ICAM-1 primer after treating the cells with ICAM-1 CRISPR/Cas9 AAV or control CRISPR/Cas9 AAV in vitro (***D***) and in vivo (***E***). Lane 1: DNA ladder. Lanes 2 and 4: control CRISPR/Cas9 AAV (control CRISPR)–treated samples showed only one band (565 bp). Lanes 3 and 5: ICAM-1 CRISPR/Cas9 AAV–treated samples showed three bands (1 uncleaved at 565 bp; 2 cleaved bands at 199 bp and 366 bp). Lane 6: No amplification without template DNA. Lane 7: Positive control is provided by the manufacturer in that three bands were detected after cleavage (750, 500, 250 bp). ***F***, ***G***, Western blot analysis of ICAM-1 in both in vitro (***F***) and in vivo (***G***), and their representative β-actin expression in hBMVECs treated with control CRISPR/Cas9, ICAM-1 CRISPR/Cas9, control siRNA, or ICAM-1 sirNA 24 h poststretch injury (***F***) and in mouse cortex tissue lysates from control CRISPR/Cas9 or ICAM-1 CRISPR/Cas9–treated control or FPI animals 14 d postinjury (***G***). Bar graphs show the quantification of ICAM-1 bands versus β-actin bands ($n = 9$–10/group). ***H***, ***I***, HRP-immunohistochemistry staining of ICAM-1 with the purple substrate (SK-4600, VectorLabs) in brain cortical tissue sections. Scale bar: 50 µm in all panels (***H***), and quantification of ICAM-1 staining in mouse cortex tissue sections analyzed using ImageJ software ($n = 10$/group) (***I***). ***J***, ***K***, mRNA quantification of ICAM-1 using qRT-PCR in cell lysates from stretch-injured and control hBMVECs treated with CRISPR/Cas9 AAV or control CRISPR/Cas9 AAV ($n = 10$/group) 24 h after 3.0 psi stretch injury (***J***) and in brain cortical tissue lysates from FPI and control animals treated with CRISPR/Cas9 AAV or control CRISPR/Cas9 AAV ($n = 9$–10/group) 14 d after 25 psi FPI (***K***). Data are shown as mean ± SD. Statistical analysis was performed by two-way ANOVA with Bonferroni's post hoc test and statistically significant values are given in each bar graph.

Mac-1 expression was very faint in *ICAM-1*$^{-/-}$ animals (Fig. 2*A*–*C*). Next, we analyzed the interaction of ICAM-1 to its receptors by immunofluorescence and co-IP. Double immunofluorescence staining results showed not only the significant expression of both ICAM-1 and LFA-1 in the FPI group compared with that in the uninjured control group ($p < 0.0001$) but the expression of ICAM-1 and LFA-1 was colocalized in brain microvessels (Fig. 2*D*,*E*). This shows the binding of ICAM-1 to its receptor LFA-1. However, ICAM-1 CRISPR/Cas9 treatments resulted in the reduced expression of both ICAM-1 and LFA-1 (Fig. 2*D*, *E*). Further, we validated the interaction of ICAM-1 with LFA-1 and Mac-1 by co-IP. Co-IP of ICAM-1 with LFA-1 or Mac-1 revealed the elevated expression of ICAM-1 along with LFA-1 and Mac-1 in the FPI group ($p < 0.0001$). In contrast, the cleavage of ICAM-1 using CRISPR/Cas9 reduced the expression of ICAM-1, LFA-1, and Mac-1 (Fig. 2*F*–*I*).

Removal of ICAM-1 reduces the transmigration of immune cells to the brain

Since we observed the interaction of ICAM-1 with its receptors LFA-1 and Mac-1, we next sought to analyze the transmigration of leukocytes to the brain. First, in an in vitro BBB model, the adhesion of immune cells was assayed by introducing Calcein-AM–labeled (a green fluorescence cell tracker) monocytes to the hBMVEC monolayer for 2 h. In stretch-injured cells, a 1.75-fold increase in Calcein-AM–labeled monocyte adhesion was observed as compared with uninjured control cells ($F_{(7,40)} = 84.37$; $p < 0.0001$; Fig. 3*A*). However, the removal of ICAM-1 using ICAM-1 CRISPR/Cas9 treatment remarkably reduced the monocyte adhesion (1.75-fold to 1.29-fold vs uninjured control cells) in stretch-injured cells ($p < 0.0001$; Fig. 3*A*). Interestingly, in uninjured control cells, we noticed that the fluorescent intensity value for the monocyte adhesion in ICAM-1 CRISPR/Cas9–treated cells was significantly less in control CRISPR/Cas9 cells ($p < 0.05$). For further validation of this observation, we used siRNA technology to silent ICAM-1 expression, and we found that the fluorescent intensity for the number of adhered monocytes was higher in stretch injury, and ICAM-1 siRNA treatment resulted in the reduction of the number of monocytes (Fig. 3*A*).

Next, we validated the regulatory role of ICAM-1 in the transmigration of immune cells to the brain in vivo. For this, first, we analyzed the endogenous expression of macrophages in the mouse brain by immunostaining CD68, a macrophage marker. Using confocal microscopy, we observed a significant number of CD68-positive cells in the cortical tissue part of the brain of the WT FPI mice ($p < 0.0001$) compared with those in uninjured controls. ICAM-1 deletion using CRISPR/Cas9 or in *ICAM-1*$^{-/-}$ mouse samples, the number of CD68-positive cells was significantly reduced ($F_{(5,42)} = 103.7$; $p < 0.0001$; Fig. 3*B*,*C*). Interestingly, in FPI WT samples, the majority of CD68-positive cells were found

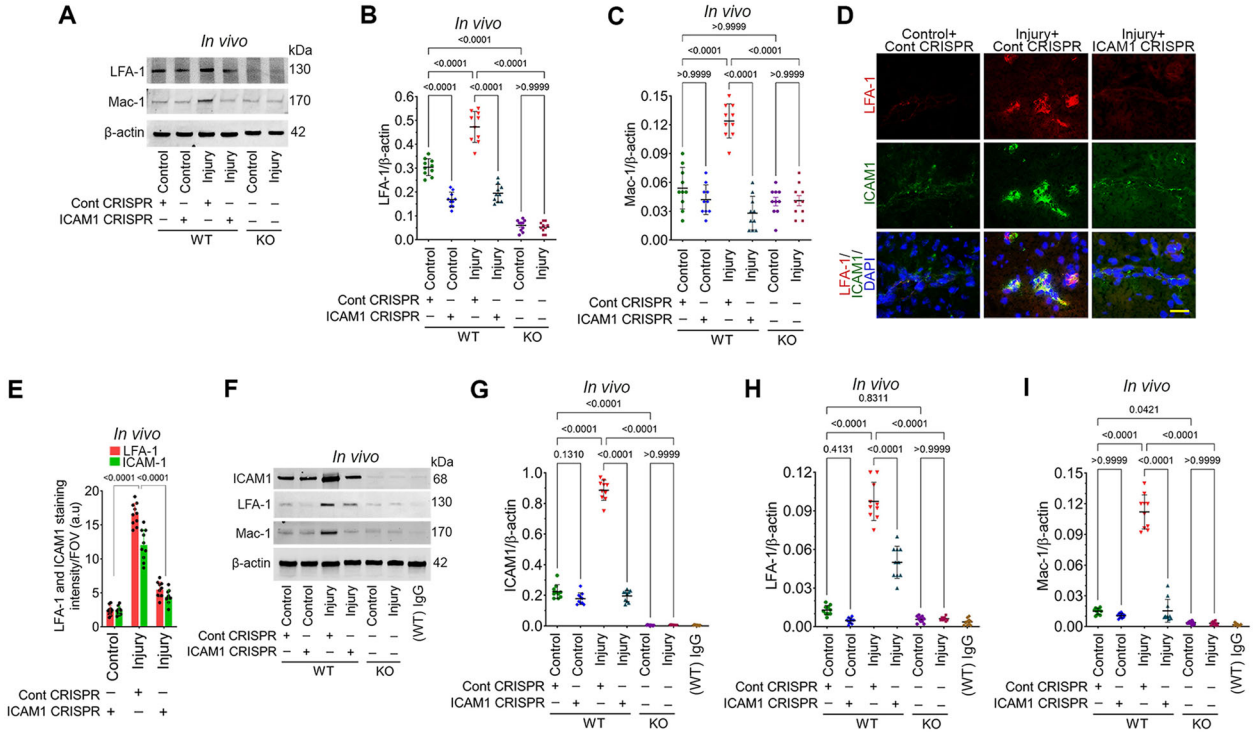

Figure 2. Deletion of ICAM-1 downregulates the expression of its receptors LFA-1 and Mac-1. ***A–C***, Western blot analysis of LFA-1 and Mac-1 and their representative β-actin expression in mouse cortex tissue lysates from FPI and control WT animals treated with control CRISPR/Cas9, or ICAM-1 CRISPR/Cas9, and from control and FPI *ICAM-1*$^{-/-}$ animals (***A***). Bar graphs show the densitometric ratio of LFA-1 (***B***) and Mac-1 (***C***) bands versus β-actin ($n = 9$–10/group). ***D***, Double immunofluorescence staining of LFA-1 (red) and ICAM-1 (green) colocalized with DAPI (blue) in control and FPI mouse brain samples treated with control CRISPR/Cas9 or ICAM-1 CRISPR/Cas9. Scale bar: 20 µm in all panels. ***E***, Quantification of LFA-1 and ICAM-1 staining in the mouse cortex tissue sections analyzed using ImageJ software ($n = 10$/group). ***F***, Co-IP of ICAM-1, LFA-1, Mac-1, and β-actin 14 d after 25 psi FPI in the tissue lysates immunoprecipitated with ICAM-1 mAb. Anti-IgG antibody was used as a negative control. ***G–I***, Bar graphs show the densitometric ratio of ICAM-1 (***G***), LFA-1 (***H***), and Mac-1 (***I***) versus β-actin bands ($n = 10$/group). Data are shown as mean ± SD. Statistical analysis was performed by one-way ANOVA (***E***) and two-way ANOVA (***B***, ***C***, ***G–I***) with Bonferroni's post hoc test and statistically significant values are given in each bar graph.

surrounding the microvessels [Fig. 3*B*; injury(WT) + Cont CRISPR panels]. To show the brain microvessel, the tissue sections were stained with vWF, an endothelial cell-specific marker. In the second experiment, we confirmed the transmigration of monocytes by infusing GFP monocytes through the common carotid artery. In this, we observed a higher number of GFP-positive monocytes just below the injury area in the FPI group than those in uninjured control samples ($F_{(5,54)} = 160.7$; $p < 0.0001$; Fig. 3*D*,*E*). In ICAM-1 CRISPR/Cas9–treated WT animals and in *ICAM-1*$^{-/-}$ animals, the number of GFP-positive monocytes was significantly reduced (Fig. 3*D*,*E*). This data shows that ICAM-1 has a significant role in the transmigration of immune cells following TBI.

Removal of ICAM-1 protects the blood–brain barrier

A distinctive phenotype of BBB endothelial cells is characterized by the presence of tight junctions (TJs) and the development of certain polarized transport mechanisms (Persidsky et al., 2006). Changes in TJ structure and integrity have a substantial impact on BBB characteristics, especially in barrier permeability. To determine the role of ICAM-1 in BBB integrity after TBI, we examined various crucial BBB proteins such as occludin, claudin-5, JAM-a, N-cadherin, and connexin-43 in both in vitro stretch injury model and in vivo FPI model. First, we evaluated the protein expression of two important TJ proteins occludin and claudin-5, which are crucial for barrier functionality. Western blotting results showed that stretch injury caused a significant decrease in the expression of occludin (reduced to one-fourth) and claudin-5 (reduced to one-fifth) compared with the uninjured control group (occludin: $F_{(7,40)} = 1.912$, $p < 0.0001$; claudin-5: $F_{(7,40)} = 2.325$, $p < 0.0001$), whereas the cells treated with ICAM-1 CRISPR/Cas9 or ICAM-1 siRNA showed an abrupt increase in the expression of both proteins compared with control CRISPR/Cas9 or control siRNA-treated stretch-injured cells ($p < 0.05$; Fig. 4*A*,*B*). Similarly, since JAM-a (a junctional adhesion molecule that is involved in facilitating the assembly of TJ components; Bazzoni, 2011), N-cadherin (an adherent junctional protein connected to pericytes; Bhowmick et al., 2019b), and connexin-43 (a member of transmembrane proteins that form gap junctions) have significant roles in maintaining the BBB integrity (Zhao et al., 2015), next we analyzed the role of ICAM-1 in the expression of these three proteins by Western blotting. As we previously reported in mice (Bhowmick et al., 2019b), the expression of JAM-a, N-cadherin, and connexin-43 was significantly reduced in the stretch-injured cells compared with that in the uninjured control cells (JAM-a: $F_{(7,40)} = 49.28$; $p < 0.0001$; N-cadherin: $F_{(7,40)} = 14.5$, $p < 0.0001$; and connexin-43: $F_{(7,40)} = 21.56$, $p < 0.0001$); however, the stretch-injured cells treated with ICAM-1 CRISPR/Cas9 or ICAM-1 siRNA exhibited improved expression of JAM-a, N-cadherin, and connexin-43 compared with control CRISPR/Cas9 or control siRNA-treated injured cells ($p < 0.01$; Fig. 4*A–D*).

Next, in animals, we confirmed the changes of these BBB proteins and validated the regulatory role of ICAM-1 in the expression of these proteins after TBI. First, when we examined the expression level of occludin and claudin-5 in injured animals, we observed a significant decrease in the expression (reduced

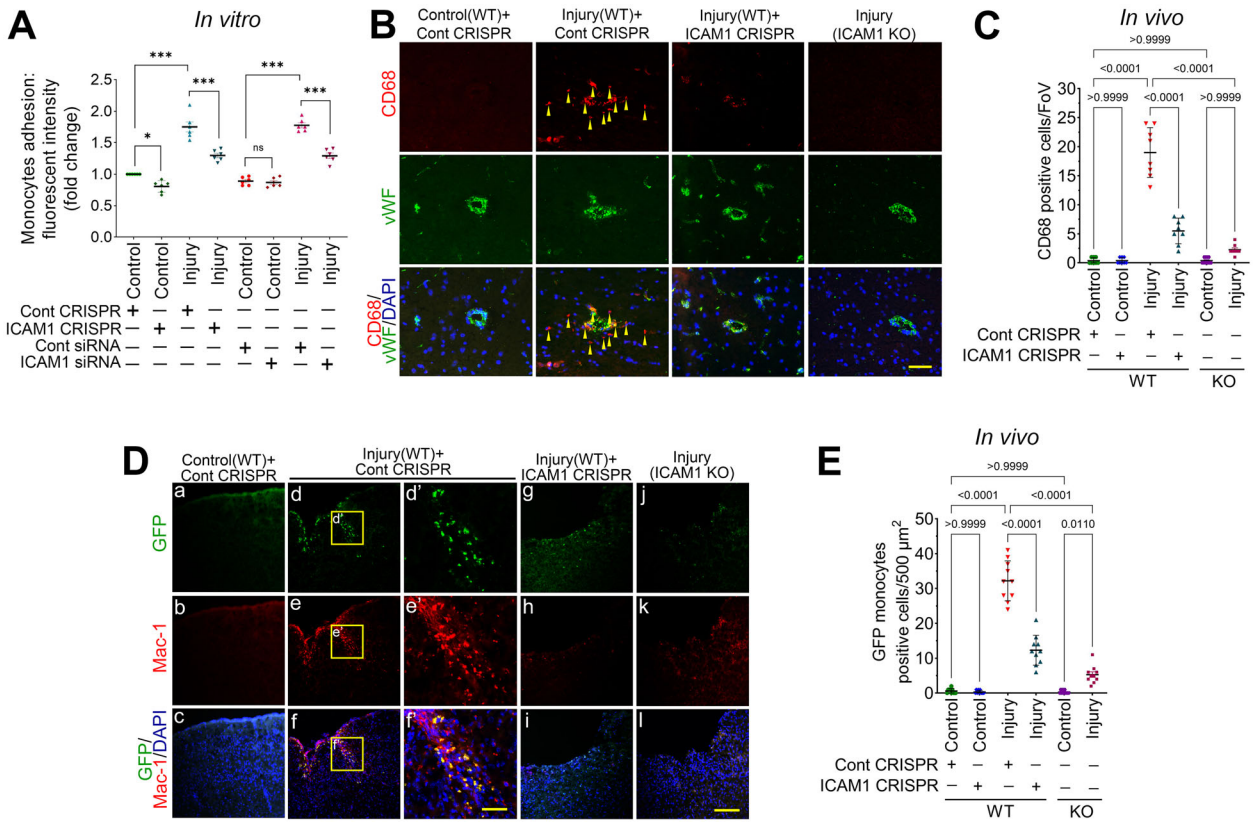

Figure 3. Deletion of ICAM-1 attenuates the transmigration of leukocytes to the brain after TBI. ***A***, Analysis of adhesion of monocytes to the monolayer of hBMVECs (the in vitro model of BBB). Adhesion of monocytes to the monolayer of hBMVECs after treatment of hBMVECs with control CRISPR/Cas9, ICAM-1 CRISPR/Cas9, control siRNA, or ICAM-1 siRNA. Data are expressed as fold difference from control (uninjured) cells treated with control CRISPR/Cas9; $n = 6$/group. ***B***, ***C***, Confocal microscopy of immunostaining of macrophage marker CD68 (red staining and yellow arrowheads) and endothelial cell marker vWF (green) colocalized with DAPI (blue). Scale bar: 40 µm in all panels (***B***) and quantification of number of CD68-positive cells analyzed using ImageJ software ($n = 8$–9/group) (***C***). ***D***, Transmigration of leukocyte analysis by infusing cultured GFP monocytes (green) through the common carotid artery of mouse and colocalized with immunostaining images of Mac-1 (red) and DAPI (blue). Panels d′, e′, and f′ are selected and enlarged areas of d, e, and f panels. Scale bars: 400 µm in a–l panels and 80 µm in d′, e′, and f′ panels. In f′ panel, the colocalized yellow cells are infused GFP cells stained with Mac-1; and red stained cells (Mac-1 alone) are endogenous blood cells. ***E***, Quantitative analysis of the number of GFP/Mac-1–positive cells. Data are shown as mean ± SD. *$p < 0.05$, **$p < 0.01$, and ***$p < 0.001$ are statistically significant. Statistically significant values are given in ***C*** and ***E*** bar graphs. Statistical analysis was performed by one-way ANOVA (***A***) and two-way ANOVA (***C*** and ***E***) with the Bonferroni's post hoc test.

to one-half) in WT FPI mice compared with that in uninjured control WT animals (occludin: $F_{(5,54)} = 186.4$, $p < 0.0001$; claudin-5: $F_{(5,54)} = 45.6$, $p < 0.0001$; Fig. 4*E*,*F*). Deletion of ICAM-1 using CRISPR/Cas9 protected the expression level of occludin and claudin-5 in FPI samples ($p < 0.0001$). Similarly, in FPI *ICAM-1*$^{-/-}$ mice, the expression of occludin and claudin-5 was not affected (Fig. 4*E*,*F*). A similar trend of results was observed in JAM-a, N-cadherin, and connexin-43 where it was reduced to one-third in JAM-a, one-half in N-cadherin, and one-fifth in connexin-43 in FPI samples compared with that in uninjured controls ($p < 0.0001$); however, the expression of N-cadherin was less when compared to the cell culture samples (Fig. 4*E*–*H*). Interestingly, in *ICAM-1*$^{-/-}$ samples and ICAM-1 CRISPR/Cas9–treated FPI samples, the expression of JAM-a, N-cadherin, and connexin-43 was not significantly affected (Fig. 4*E*–*H*).

Disruption of BBB integrity as a result of brain injury was assessed by the permeability of NaFl and EB tracers across the BBB (Abdul-Muneer et al., 2013; Bhowmick et al., 2019b). FPI in mice greatly increased the permeability of small molecular weight NaFl (MW = 376 kDa; ∼2 times) and large molecular weight tracer EB (MW = 961 kDa; ∼2.4 times) across the BBB compared with respective uninjured controls (NaFl: $F_{(5,54)} = 53.18$, $p < 0.0001$; EB: $F_{(5,54)} = 100.9$, $p < 0.0001$; Fig. 4*I*,*J*), which correlated with the enhanced immune cell adhesion and infiltration into the brain. However, ICAM-1 CRISPR/Cas9–treated FPI mice showed a significantly reduced value of BBB permeability to these two tracers compared with control CRISPR/Cas9–treated controls ($p < 0.0001$), whereas FPI *ICAM-1*$^{-/-}$ mice showed a significantly reduced permeability of NaFl and EB compared with injured WT animals ($p < 0.0001$; Fig. 4*I*,*J*).

Paxillin–FAK pathway regulates the transmigration of leukocytes to the brain

Next, we thrived to investigate the mechanisms of transmigration of leukocytes to the brain after TBI. First, we analyzed the role of paxillin–FAK signaling in regulating ICAM-1-induced transmigration of leukocytes to the brain. For this, we treated the hBMVEC cultures with ICAM-1 CRISPR/Cas9, control CRISPR/Cas9, ICAM-1 siRNA, and control siRNA 30 min prior to stretch injury and analyzed the expression level of paxillin and FAK and their phosphorylated forms by Western blotting. In stretch-injured hBMVECs, the levels of p-paxillin ($F_{(7,40)} = 0.637$; $p < 0.001$) and p-FAK ($F_{(7,40)} = 1.476$; $p < 0.0001$) immunoreactive proteins were significantly increased when compared with those in uninjured control cells, whereas deleting or silencing of ICAM-1 using CRISPR/Cas9 or siRNA blocked the phosphorylation of paxillin and FAK proteins

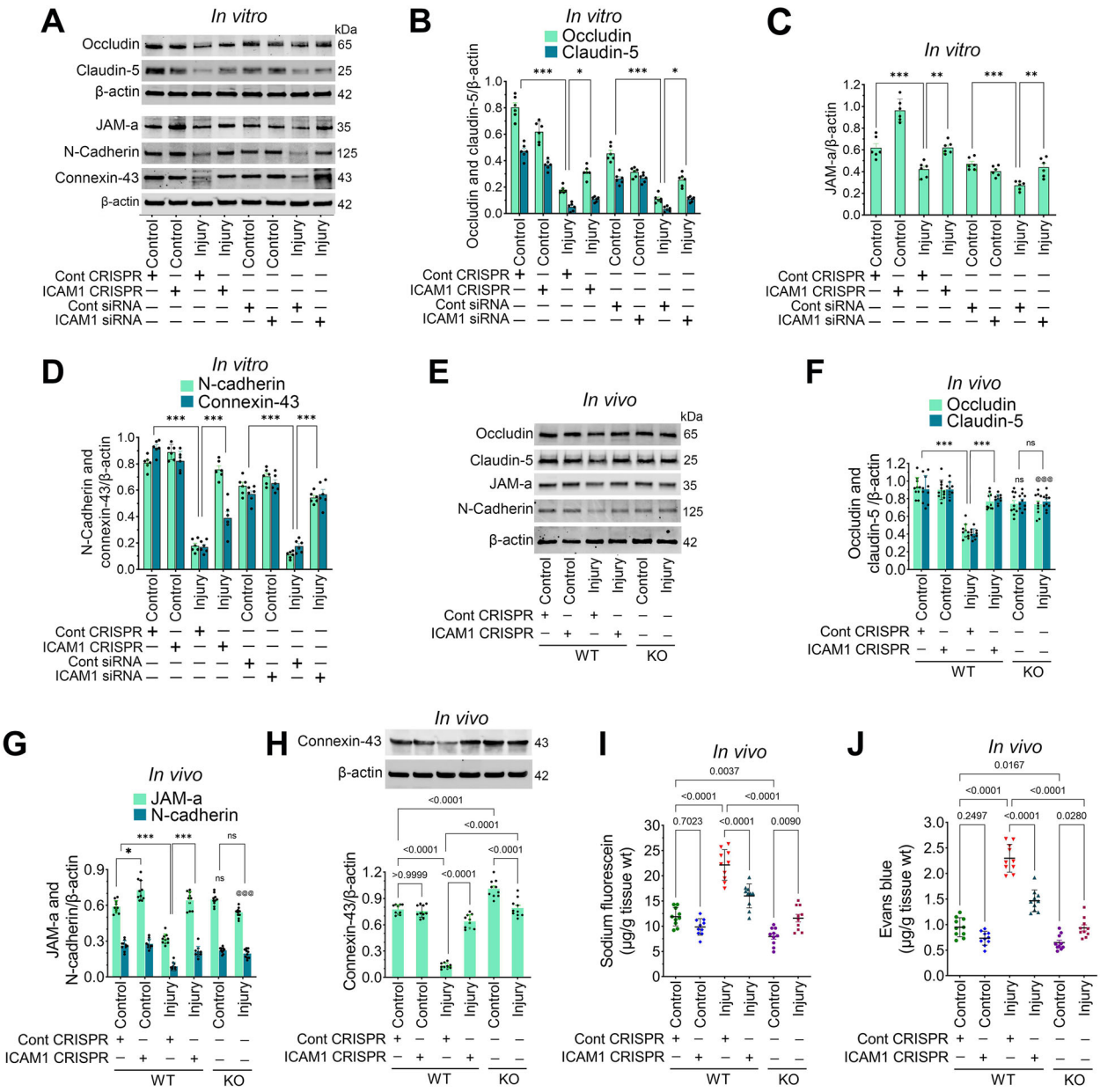

Figure 4. Deletion of ICAM-1 protects the TBI-induced blood–brain barrier damage. ***A–D***, Western blot analysis of occludin, claudin-5, JAM-a, N-cadherin, connexin-43, and their representative β-actin expression in hBMVECs treated with control CRISPR/Cas9, ICAM-1 CRISPR/Cas9, control siRNA, or ICAM-1 sirNA 24 h poststretch injury. Bar graphs show the quantification of occludin and claudin-5 (***B***), JAM-a (***C***), and N-cadherin and connexin-43 (***D***) bands versus β-actin bands ($n = 6$/group). ***E–H***, Western blot analysis of occludin, claudin-5, JAM-a, N-cadherin, connexin-43, and their representative β-actin expression in brain cortex tissue lysates of control and FPI WT mouse treated control CRISPR/Cas9, or ICAM-1 CRISPR/Cas9, and untreated control and FPI *ICAM-1*$^{-/-}$ mice. Bar graphs show the quantification of occludin and claudin-5 (***F***), JAM-a and N-cadherin (***G***), and connexin-43 (***H***) bands versus β-actin bands ($n = 10$/group). ***I***, ***J***, Graphical representation of in vivo permeability to show the leakage of sodium fluorescein (NaFl, 5 µM; ***I***) and EB (5 µM; ***J***) of control and FPI WT mouse treated control CRISPR/Cas9, or ICAM-1 CRISPR/Cas9, and untreated control and FPI *ICAM-1*$^{-/-}$ mice. Data are shown as mean ± SD. Statistically significant: $^{*}p < 0.05$, $^{**}p < 0.01$, $^{***}p < 0.001$ as marked, and $^{@@@}p < 0.001$. $^{@@@}p < 0.001$ versus WT FPI group. Statistically significant values are given in ***H–J*** bar graphs. Statistical analysis was performed by one-way ANOVA (***B–D***) and two-way ANOVA (***F–J***) with Bonferroni's post hoc test.

(Fig. 5*A*,*B*). However, there was no perceptible change in the levels of paxillin and FAK proteins (Fig. 5*A*,*B*). The significant reduction in p-paxillin and p-FAK levels with ICAM-1 inhibition shows ICAM-1 is linked with the paxillin–FAK pathway and has a significant role in the transmigration of immune cells after TBI. Further, in WT and *ICAM-1*$^{-/-}$ animals, we validated the changes in the protein expression of p-paxillin and p-FAK in the cortical brain tissue lysates beneath the site of injury from FPI mouse samples and compared them with uninjured controls. Here too, the expression of p-paxillin ($F_{(5,54)} = 0.964$; $p < 0.0001$) and p-FAK ($F_{(5,54)} = 0.136$; $p < 0.0001$) were higher in FPI animals than that in uninjured controls in both WT and *ICAM-1*$^{-/-}$ (Fig. 5*C*,*D*). However, as we expected, the levels of p-paxillin and p-FAK were significantly reduced in ICAM-1 CRISPR/Cas9–treated WT FPI animal samples as compared with those in untreated WT FPI animal samples ($p < 0.0001$), and the levels of paxillin and FAK remained unchanged (Fig. 5*C*,*D*).

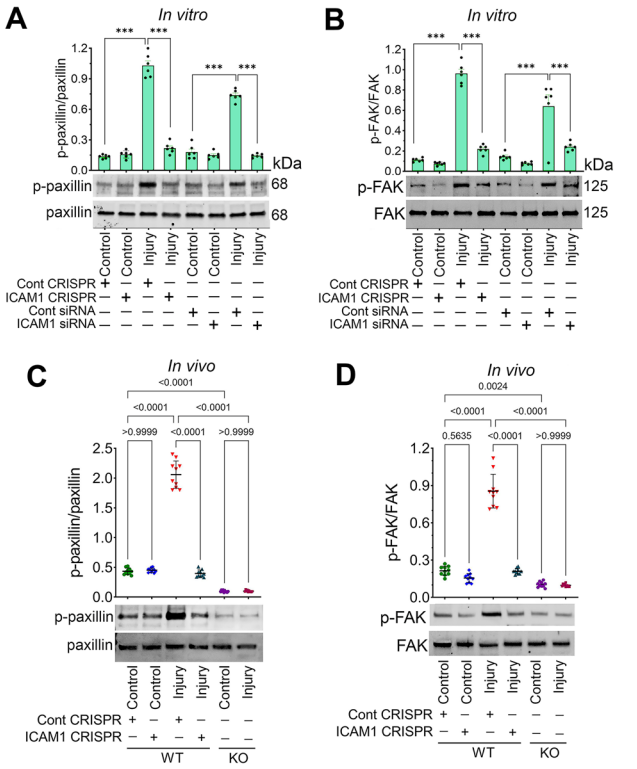

Figure 5. ICAM-1–induced transmigration of leukocytes is dependent on the paxillin/FAK pathway. ***A, B***, Western blot analysis of paxillin/p-paxillin (***A***) and FAK/p-FAK (***B***) and their representative β-actin expression in stretch-injured and control hBMVECs treated with control CRISPR/Cas9, ICAM-1 CRISPR/Cas9, control siRNA, or ICAM-1 siRNA. Bar graphs show the densitometric ratio of paxillin and p-paxillin (***A***) and FAK and p-FAK (***B***) versus β-actin bands in hBMVECs ($n = 10$/group). ***C***, ***D***, Western blot analysis of paxillin/p-paxillin (***C***) and FAK/p-FAK (***D***) and their representative β-actin expression in brain cortex tissue lysates of control and FPI WT mouse treated control CRISPR/Cas9, or ICAM-1 CRISPR/Cas9, and untreated control and FPI *ICAM-1*$^{-/-}$ mice. Bar graphs show the densitometric ratio of paxillin and p-paxillin (***C***) and FAK and p-FAK (***D***) versus β-actin bands in mouse brain cortex tissue lysates ($n = 10$/group). Data are shown as mean ± SD. *$p < 0.05$ and ***$p < 0.001$ are statistically significant. Statistical analysis was performed by one-way ANOVA (***A***, ***B***) and two-way ANOVA (***C***, ***D***) with Bonferroni's post hoc test.

Transmigration of leukocytes is regulated by the Rho GTPase pathway

Paxillin plays a central role in coordinating the spatial and temporal action of the Rho family of small GTPases, which regulate the actin cytoskeleton by recruiting an array of GTPase activators, suppressors, and effector proteins to cell adhesions (Hodge and Ridley, 2016). Activation of Rho GTPase is a continuous mechanism of ICAM-1–induced transmigration of immune cells. After analyzing the expression level and phosphorylation of paxillin, next we analyzed the expression of Src and its phosphorylated form. Like FAK, Src is also involved in the phosphorylation of paxillin, and to demonstrate the phosphorylation of Src, we analyzed the expression level of p-Src by Western blotting. In our stretch-injured samples, we observed a significantly high level of p-Src compared with that in uninjured control samples ($F_{(7,40)} = 0.185$; $p < 0.0001$), and ICAM-1 CRISPR/Cas9 or ICAM-1 siRNA treatment significantly reduced the protein content of p-Src in stretch-injured samples ($p < 0.0001$; Fig. 6*A*,*B*).

To determine the role of the Rho GTPase pathway in ICAM-1–induced transmigration of leukocytes after TBI, we analyzed the expression of different molecules of the Rho GTPase family including Rac1, RhoA, and Cdc42 with or without treating ICAM-1 CRISPR/Cas9 or ICAM-1 siRNA in hBMVECs. In stretch-injured hBMVECs, the expression of p-Rac1 ($F_{(7,40)} = 0.749$; $p < 0.0001$) was significantly increased when compared with that in uninjured control cells, whereas the phosphorylation of Rac1 protein was inhibited when deleting or silencing of ICAM-1 using CRISPR/Cas9 or siRNA (Fig. 6*A*,*C*). However, the expression of the Rac1 protein was not changed (Fig. 6*A*,*C*). Similarly, we analyzed the expression level of the other two important members of the Rho GTPase pathway, Cdc42 and RhoA, that are involved in cellular functions such as cell migration, endocytosis, and actin organization (Etienne-Manneville and Hall, 2002). A remarkable highly significant expression of Cdc42 and RhoA was found in stretch-injured cell samples compared with that in uninjured controls ($F_{(7,40)} = 4.904$; $p < 0.0001$). As predicted, ICAM-1 CRISPR/Cas9 or ICAM-1 siRNA treatment significantly reduced the expression of Cdc42 and RhoA in stretch-injured samples ($p < 0.0001$; Fig. 6*D*,*E*).

Next, in animals, we validated the role of Src and Rho GTPase molecules in the regulatory mechanisms of ICAM-1–induced transmigration of leukocytes after TBI. First, when we examined the expression level of Src and p-Src in FPI animals, we observed a significant increase in p-Src expression (~8 times fold) in WT FPI mice compared with that in uninjured control WT animals ($F_{(5,54)} = 0.698$; $p < 0.0001$). Removal of ICAM-1 using CRISPR/Cas9, the expression level of p-Src was highly reduced in FPI samples compared with that in untreated FPI samples ($p < 0.0001$). However, in *ICAM-1*$^{-/-}$ mice, a negligible level of p-Src protein was observed in both FPI and uninjured samples (Fig. 6*F*,*G*). A similar trend of results was observed in p-Rac1 in both FPI and uninjured WT and *ICAM-1*$^{-/-}$ mice ($F_{(5,54)} = 0.255$; $p < 0.0001$; Fig. 6*F*,*H*). As observed in cells, the expression of Src and Rac1 did not change in FPI samples of WT and *ICAM-1*$^{-/-}$ mice (Fig. 6*F*–*H*). Likewise, a similar trend in the expression of Cdc42 and RhoA was observed where it was increased to ~6 times ($F_{(5,54)} = 9.652$; $p < 0.0001$) in FPI samples when compared with that in uninjured controls (Fig. 6*I*). Interestingly, when we removed the ICAM-1 using CRISPR/Cas9, the expression of Cdc42 and RhoA substantially reduced ($p < 0.0001$), whereas, in *ICAM-1*$^{-/-}$ samples, a faint expression of Cdc42 and RhoA was observed (Fig. 6*I*).

Removal of ICAM-1 protects the brain from TBI-induced neuroinflammation

Since VEGF-A has a significant role in neuroinflammation and cell migration (Abdul Muneer et al., 2012), in the beginning, we analyzed if ICAM-1 has any role in the induction of VEGF-A in stretch-injured cells by ELISA. Even though the level of VEGF-A was increased significantly in stretch-injured samples compared with that in uninjured cells ($F_{(7,40)} = 27.5$; $p < 0.0001$), the deletion or silencing of ICAM-1 by treating ICAM-1 CRISPR/Cas9 or ICAM-1 siRNA did not affect the level of VEGF-A in stretch-injured cells (Fig. 7*A*). This data shows that ICAM-1 has no role in inducing VEGF-A. Next, since the neutrophil chemotactic factor, CXCL-8 also known as IL-8, induces chemotaxis in primary neutrophils and other granulocytes causing them to migrate toward the site of infection (Meliton et al., 2010), we analyzed the expression level of CXCL-8 (IL-8) by ELISA. A 2.5-fold increase in CXCL-8 was observed in stretch-injured samples compared with that in uninjured controls; however, ICAM-1 CRISPR/Cas9 or ICAM-1 siRNA treatment significantly reduced the level of CXCL-8 in stretch-injured cells ($F_{(7,40)} = 27.91$; $p < 0.0001$; Fig. 7*B*). Similarly, when we quantified two common proinflammatory cytokines, IL-1β and TNF-α, we

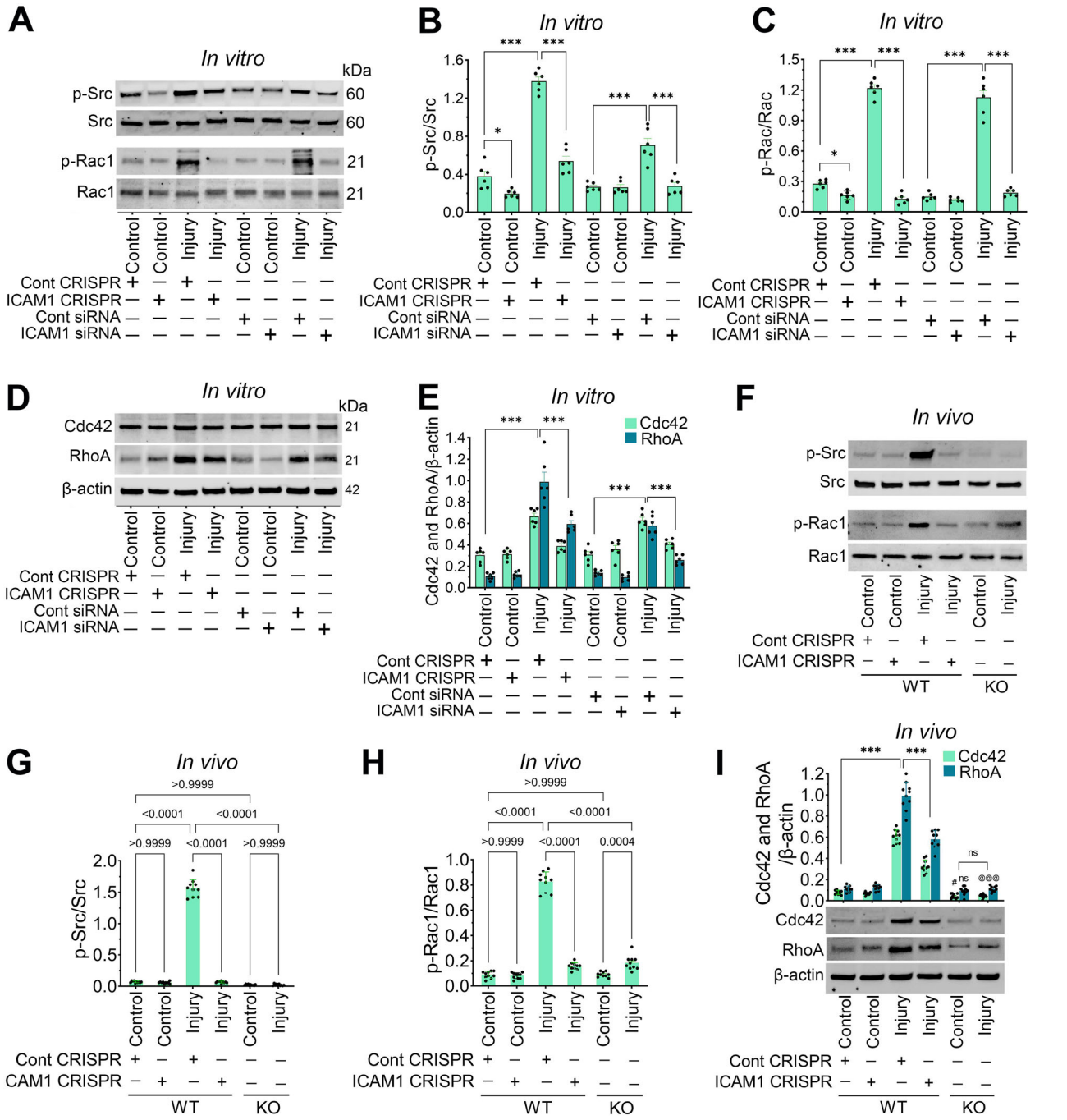

Figure 6. ICAM-1–induced transmigration of leukocytes is regulated by the Rho GTPase pathway. ***A–C***, Western blot analysis of p-Src, Src, p-Rac1, Rac1, and their representative β-actin expression in control and stretch-injured hBMVECs treated with control CRISPR/Cas9, ICAM-1 CRISPR/Cas9, control siRNA, or ICAM-1 siRNA. Bar graphs show the quantification of p-Src, Src, p-Rac1, and Rac1 in hBMVECs. Bar graphs (***B***, ***C***) show the densitometric ratio of p-Src and Src (***B***) and p-Rac1 and Rac1 (***C***) versus β-actin bands in hBMVECs ($n = 10$/group). ***D***, ***E***, Western blot analysis of Cdc42 and RhoA and their representative β-actin expression in hBMVECs lysates (***D***). Bar graph (***E***) shows the densitometric ratio of Cdc42 and RhoA to β-actin bands ($n = 10$/group). ***F***, ***H***, Western blot analysis of p-Src, Src, p-Rac1, Rac1, and their representative β-actin expression in control and FPI WT mouse's cortex tissue lysates treated with control CRISPR/Cas9, or ICAM-1 CRISPR/Cas9, and untreated control and FPI *ICAM-1*$^{-/-}$ animals (***F***). Bar graphs (***G***, ***H***) show the densitometric ratio of p-Src and Src (***G***) and p-Rac1 and Rac1 (***H***) versus β-actin bands in mouse cortex tissue lysates ($n = 10$/group). ***I***, Western blot analysis of Cdc42 and RhoA and their representative β-actin expression in mouse cortex tissue lysates. Bar graph (***I***) shows the densitometric ratio of Cdc42 and RhoA versus β-actin bands in mouse cortex tissue lysates ($n = 10$/group). Data are shown as mean ± SD. *$p < 0.05$ and ***$p < 0.001$ are statistically significant. Statistical analysis was performed by one-way ANOVA (***B***, ***C***, and ***E***) and two-way ANOVA (*G–I*) with the Bonferroni's post hoc test.

observed a similar trend as we found for CXCL-8 (IL-1β: $F_{(7,40)} = 51.24$, $p < 0.0001$ and TNF-α: $F_{(7,40)} = 33.39$, $p < 0.0001$; Fig. 7*A*, *B*). These data show that ICAM-1 has a significant role in inducing CXCL-8, IL-1β, and TNF-α in stretch-injured cells.

Next, we validated the expression levels of these four inflammatory markers in animal samples including blood plasma and cortex tissue lysates. The quantification of VEGF-A in blood plasma and cortex tissue lysates shows significantly high (three-fold in blood plasma and 2.5-fold in the cortex) in FPI animal samples compared with that in uninjured controls (blood plasma: $F_{(5,54)} = 67.65$, $p < 0.0001$; cortex: $F_{(5,54)} = 27.1$, $p < 0.0001$). Interestingly, as we found in cell culture samples,

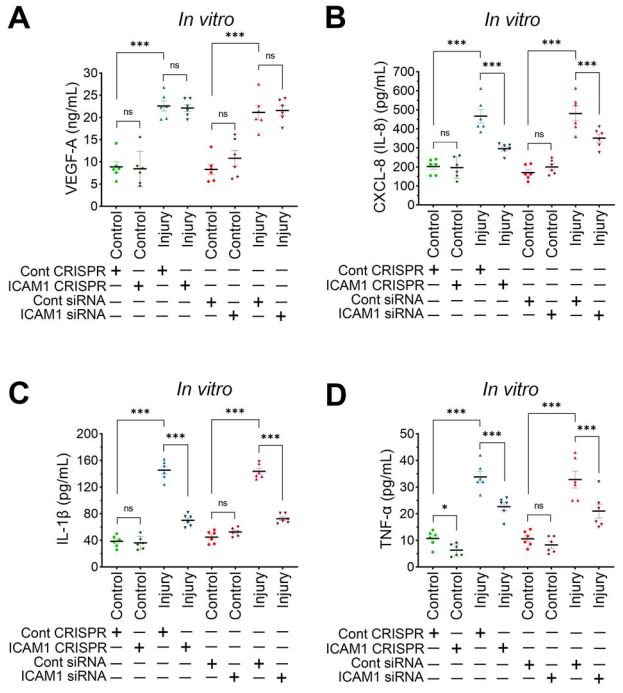

Figure 7. ICAM-1 activates chemokines and cytokines in vitro after stretch injury in hBMVECs. ***A–D***, ELISA quantification of VEGF-A (***A***), CXCL-8 (IL-8; ***B***), IL-1β (***C***), and TNF-α (***D***) in the cell culture supernatant of control and stretch-injured hBMVECs treated with control CRISPR/Cas9, ICAM-1 CRISPR/Cas9, control siRNA, or ICAM-1 siRNA. Data are shown as mean ± SD and $n = 6$/group. $^{*}p < 0.05$ and $^{***}p < 0.001$ are statistically significant. Statistical analysis was performed by one-way ANOVA with Bonferroni's post hoc test. ns, not significant.

ICAM-1 CRISPR/Cas9 or ICAM-1 siRNA treatment did not affect the level of VEGF-A in both blood plasma and cortex tissue lysates (Fig. 8*A*,*B*). Next, when we estimated the quantity of CXCL-8, a significant increase was noticed in blood plasma and cortex samples of FPI animals compared with that of uninjured controls; however, ICAM-1 CRISPR/Cas9 or ICAM-1 siRNA treatment significantly reduced the level of CXCL-8 in blood plasma and cortex samples of FPI animals (blood plasma: $F_{(5,54)} = 126.5$, $p < 0.0001$; cortex: $F_{(5,54)} = 447.7$, $p < 0.0001$; Fig. 8*C*,*D*). Similarly, when we estimated the level of other active proinflammatory cytokines such as IL-1β and TNF-α in the blood plasma and cortex tissue lysates by ELISA, we found a significant increase in the level of these proteins in blood plasma and cortex samples of FPI animals compared with that of uninjured controls (IL-1β: blood plasma, 3.4-fold, $F_{(5,54)} = 132.1$, $p < 0.0001$; cortex tissue, 4.8-fold, $F_{(5,54)} = 131.5$, $p < 0.0001$; and TNF-α: blood plasma, 3.5-fold, $F_{(5,54)} = 132.1$, $p < 0.0001$; cortex tissue, 6.86-fold, $F_{(5,54)} = 197$, $p < 0.0001$); however, ICAM-1 CRISPR/Cas9 or ICAM-1 siRNA treatment significantly reduced the level of IL-1β and TNF-α in FPI animal's blood plasma and cortex samples ($p < 0.0001$; Fig. 8*E*–*H*). Taken together, these data indicate that ICAM-1 has a significant role in inducing CXCL-8, IL-1β, and TNF-α after TBI.

Deletion of ICAM-1 protects the TBI victims from functional deficits

Since we previously observed ICAM-1 causes sensorimotor deficits and psychological stress following TBI (Bhowmick et al., 2021), in this study, we ought to evaluate whether deletion of ICAM-1 protects the TBI victims from sensorimotor deficits, psychological stress, and memory impairments. In sensorimotor function analysis, the rotarod test showed that deletion of ICAM-1 substantially increased the time for latency to fall from the rotarod as compared with FPI animals 7 and 14 d after ICAM-1 CRISPR/Cas9 treatment (reduced to half after 7 and 14 d; $F_{(5,48)} = 354$, $p < 0.0001$; Fig. 9*A*). We further validated the recovery from the sensorimotor function in a grid walk test. ICAM-1 deletion in FPI mice significantly reduced the grid walk time (reduced to 65%; $F_{(5,48)} = 34.56$, $p < 0.0001$) and errors (reduced to 57%; $F_{(5,48)} = 92.58$, $p < 0.0001$) to complete one grid walk length (Fig. 9*B*,*C*).

Next, for assessing psychological stress such as anxiety-like and depression-like behaviors, we used the light–dark test and sucrose preference test, respectively. In the light–dark test, *ICAM-1* deletion (in ICAM-1 CRISPR/Cas9 treatment and *ICAM-1*$^{-/-}$) causes a significant increase in latency to stay in the light chamber or the number of transition when compared with control CRISPR/Cas9 treatment and WT FPI mice ($F_{(5,48)} = 14.62$; $p < 0.0001$; Fig. 9*D*,*E*). In the sucrose preference test, although the WT FPI group showed a significant reduction in the sucrose preference to the uninjured control groups at 14 d post-TBI ($F_{(5,48)} = 32.58$; $p < 0.0001$; Fig. 9*F*), ICAM-1 CRISPR/Cas9 treatment substantially improves sucrose preference at 14 d when compared with control CRISPR/Cas9 treatment animals (Fig. 9*F*). As expected, the sucrose preference in injured *ICAM-1*$^{-/-}$ was significantly less compared with WT FPI animals (Fig. 9*F*).

Next, we assessed spatial learning and memory using the MWM test. During the spatial acquisition period, the escape latency, the time mouse took to find the hidden platform, was measured (Fig. 9*G*). For WT FPI mice, the escape latency decreased over four consecutive training trials on each experiment day with the value on the 14th day (average 27.33 s) only 47% of the value on the initial day (baseline: average 51.33 s). Comparatively, for the WT FPI group on the 14th day, it still took 78.8% of the initial latency on the baseline day (average 53.66 s) to find the hidden platform (average 42.33 s), which was 2.12-fold of the time of the WT uninjured group ($p < 0.0001$), indicating learning and memory impairment in the FPI mice (Fig. 9*G*). However, in the ICAM-1 CRISPR/Cas9–treated FPI group, the escape latency for the fourth training time on the 14th day (average, 32 s) was significantly reduced, and it was only 57.8% of the value of the initial training (average, 55.33 s; $p < 0.001$). When we compared ICAM-1 CRISPR/Cas9–treated FPI group with the control CRISPR/Cas9–treated FPI group, on the 14th day, the escape latency time was significantly less in ICAM-1 CRISPR/Cas9–treated FPI group (32 s vs 42.33 s; $p < 0.0001$). In *ICAM-1*$^{-/-}$ uninjured and FPI animals, the escape latency of the fourth training was significantly less compared with that of the baseline test; interestingly, these values are significant when compared with WT respective groups (Fig. 9*G*). The probe trials for all the experimental groups are given in Figure 9*H*. From these probe trails, we analyzed the number of hidden platform crossings and probe time. The number of hidden platform crossings showed a considerable less in the FPI group compared with that in uninjured controls (average, 4.4 vs 0.33; $F_{(5,54)} = 34.93$; $p < 0.0001$); however, as expected the number of crossings was high in ICAM-1 CRISPR/Cas9–treated FPI mice compared with that in control CRISPR/Cas9–treated FPI mice (2.4 vs 0.33; Fig. 9*I*). Interestingly, in *ICAM-1*$^{-/-}$ FPI mice, the number of crossings was significantly high when compared with that in control WT FPI mice (Fig. 9*I*). Next, the probe time was significantly high in the FPI group compared with that in uninjured controls, and ICAM-1 CRISPR/Cas9 treatment

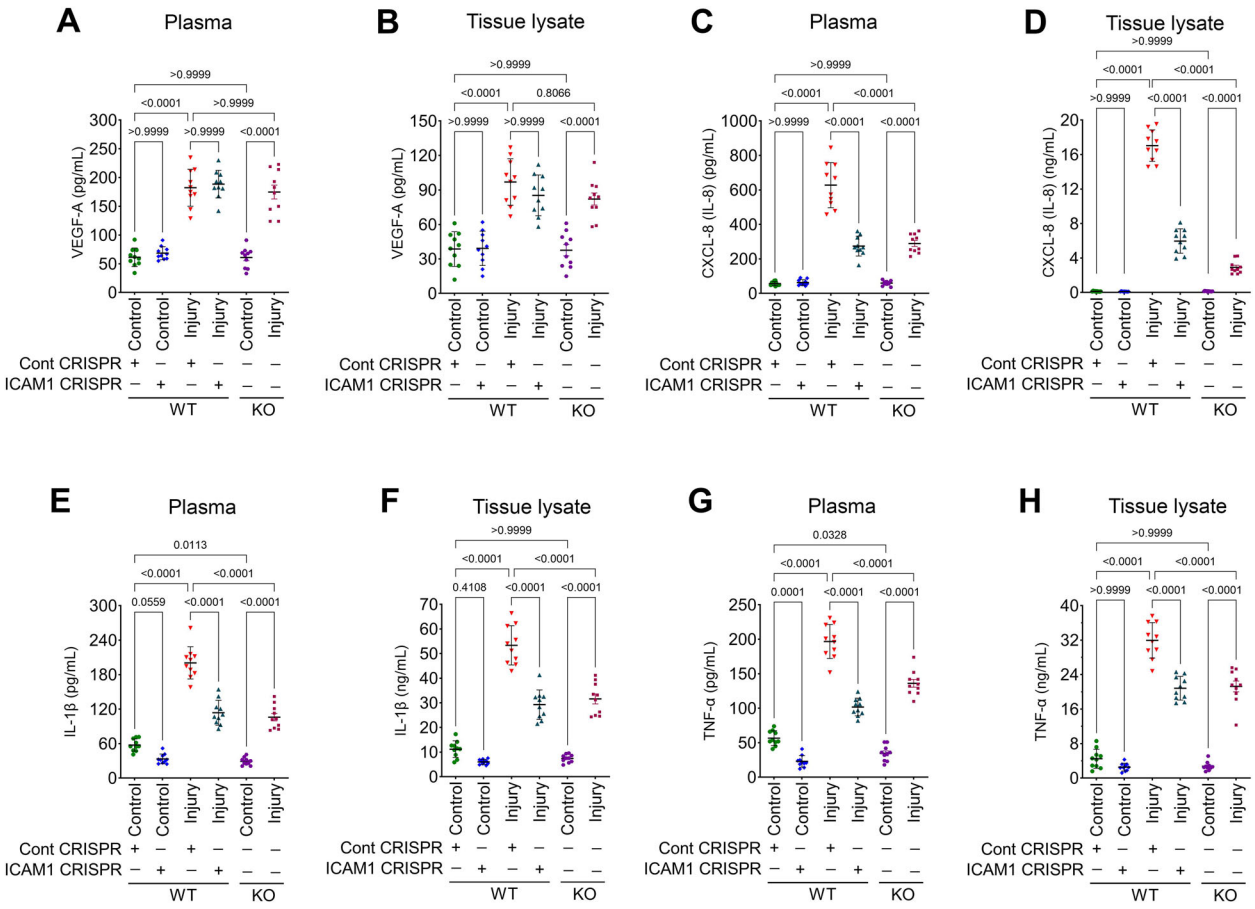

Figure 8. ICAM-1 activates chemokines and cytokines and causes neuroinflammation in animals after TBI. ***A–H***, ELISA quantification of VEGF-A (***A***, ***B***), CXCL-8 (IL-8; ***C***, ***D***), IL-1β (***E***, ***F***), and TNF-α (***G***, ***H***) in the blood plasma and brain tissue lysates, respectively, of control and FPI WT mouse treated with control CRISPR/Cas9, or ICAM-1 CRISPR/Cas9, and control and FPI *ICAM-1*$^{-/-}$ animals. Bar graphs (***A–H***) show the quantification of ELISA. Data are shown as mean ± SD and $n = 6$/group. *$p < 0.05$ and ***$p < 0.001$ are statistically significant. Statistical analysis was performed by two-way ANOVA with Bonferroni's post hoc test. ns, not significant.

reduced it ($F_{(5,54)} = 46.52$; $p < 0.0001$; Fig. 9*J*). These data indicate that ICAM-1–induced brain damage is involved in regulating sensorimotor, depression, and anxiety-like psychological stress and cognitive functions behavior.

Discussion

Inflammatory leukocyte adhesion and transmigration events and their impact on neuroinflammation and cognitive impairments are reported in TBI incidents (Schwarzmaier et al., 2013; Bhowmick et al., 2021). Though several authors reported the role of two adhesion molecules, ICAM and VCAM in the transmigration of leukocytes to the brain, the exact mechanisms or the downstream pathways of the transmigration process are not yet established in TBI. We previously reported that ICAM-1 plays a significant role in the transmigration of leukocytes to the brain and neuroinflammatory cascades that lead to sensorimotor deficits and psychological stress (Bhowmick et al., 2021). In this study, we showed the role of ICAM-1 in the transmigration of leukocytes and neuroinflammation by regulating paxillin/FAK and Rho GTPase pathways after TBI in vitro utilizing stretch injury model in hBMVEC and in vivo in FPI model in mice. We deleted ICAM-1 and validated our results by treating the cells and animals with ICAM-1 CRISPR/Cas9 and in *ICAM-1*$^{-/-}$ mice.

ICAM-1 is a transmembrane endothelial cell adhesion molecule that belongs to the supergene family of immunoglobulins (Dietrich, 2002; Frank and Lisanti, 2008). Changes in the expression of ICAM-1 have been reported in various models of TBI. In mouse models of controlled cortical impact (Muradashvili et al., 2015; Baban et al., 2021), weight drop (Jin et al., 2008), and FPI (Witcher et al., 2021), and repetitive head impacts in humans (Kirsch et al., 2023) and cortical contusion model in rats (Isaksson et al., 1997), an elevation of endothelial expression of ICAM-1 in brain cortical vessels was reported. In the same model, Whalen et al. reported the role of ICAM-1 in neutrophil accumulation, lesion volume, and impairment of cognitive functions using *ICAM-1*$^{-/-}$ mice (Whalen et al., 1999). ICAM-1–induced inflammatory leukocyte adhesion, and transmigration processes are carried out when ICAM-1 binds with its receptors LFA-1 (CD11a/CD18) and Mac-1 (CD11b/CD18) present in leukocytes (Kelly et al., 1996). In our previous study, we reported that a strong cooperative interaction of ICAM-1 with its receptors LFA-1 and Mac-1 exists following injury, and this cooperative interaction plays a major role in downstream neuroinflammatory and pathophysiology outcomes apart from leukocyte transmigration (Bhowmick et al., 2021). This strong interaction of ICAM-1 with its receptors LFA-1 and Mac-1 was validated in this study and confirmed the role in the transmigration of leukocytes to the brain. Here, in co-IP, we observed that the deletion of ICAM-1 compromised the binding of ICAM-1 with its receptors because, in the absence of ICAM-1, the receptors LFA-1 and Mac-1 were less activated. We validated these findings in *ICAM-1*$^{-/-}$ animals.

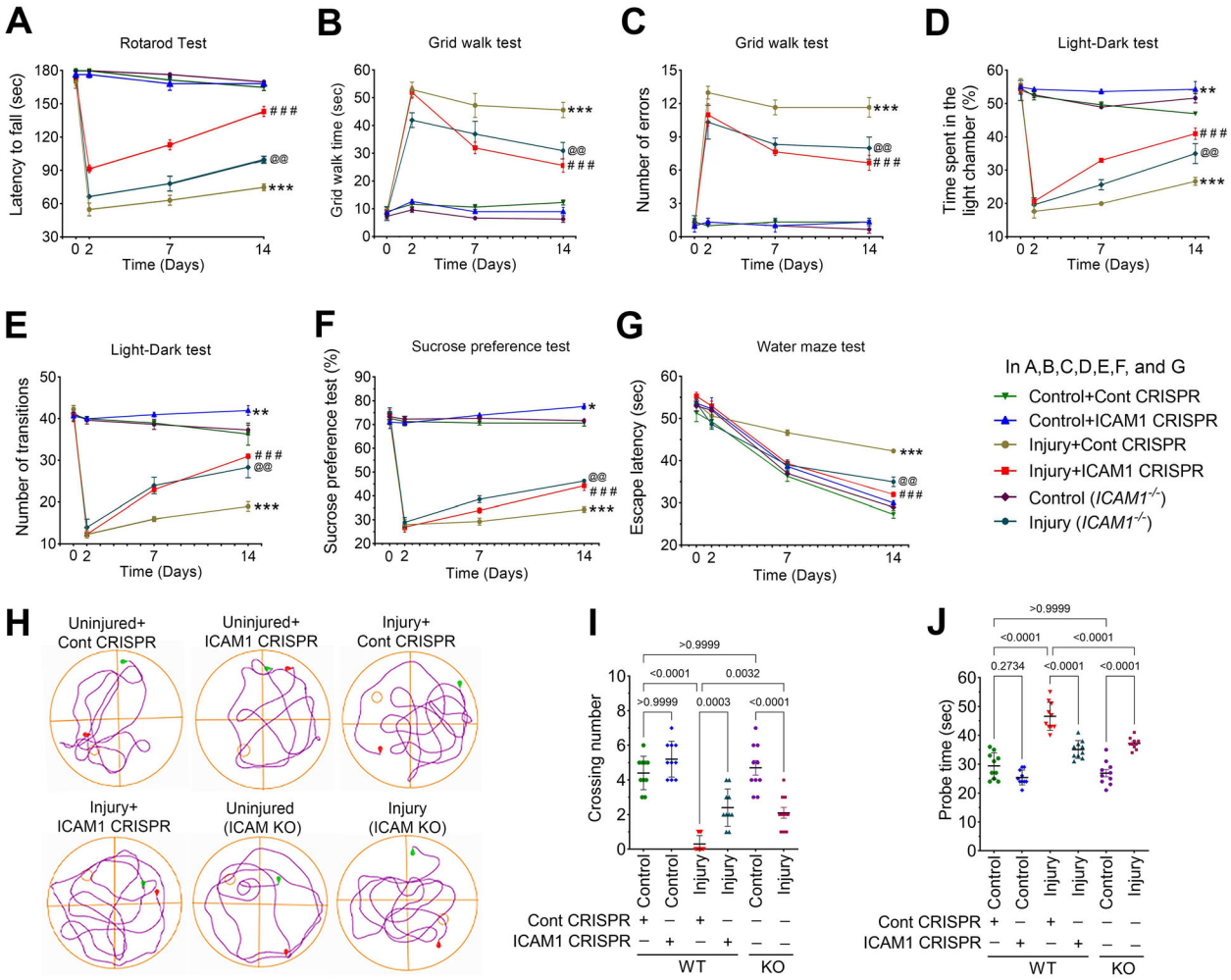

Figure 9. ICAM-1 deletion promotes sensorimotor and cognitive functions and reduces psychological stress after TBI. ***A***, Latency to fall time in rotarod was examined in WT and *ICAM-1*$^{-/-}$ mice at baseline (0 d), 2, 7, and 14 d after 25 psi FPI ($n = 9$–10/group). ***B***, ***C***, The grid walk analysis (the time to finish a grid walk; ***B***), and the number of grid walk errors (***C***) were monitored in WT and *ICAM-1*$^{-/-}$ mice at baseline (0 d), 2, 7, and 14 d after 25 psi FPI ($n = 9$–10/group). ***D***, ***E***, The light–dark box test for anxiety-like behavior expressed as percentage of time spent exploring the light chamber (***D***) and the number of transitions between the chambers (***E***) monitored at baseline (0 d), 2, 7, and 14 d after 25 psi FPI in WT and *ICAM-1*$^{-/-}$ mice subjected to 25 psi FPI ($n = 10$/group). ***F***, The sucrose preference test for depression behavior was calculated as a percentage of the volume of sucrose intake over the total volume of fluid intake at baseline (0 d), 2, 7, and 14 d after 25 psi FPI in WT and *ICAM-1*$^{-/-}$ mice subjected to 25 psi FPI ($n = 10$/group). ***G–J***, The performance of the mice in the MWM test. ***G***, The escape latencies in the six experimental groups over four consecutive trials at baseline (0 d), 2, 7, and 14 d of the spatial acquisition session. ***H***, Representative swimming paths of the control and FPI WT and *ICAM-1*$^{-/-}$ mice during the probe trial. WT mice were treated with control CRISPR/Cas9 or ICAM-1 CRISPR/Cas9 1 h after FPI. ***I***, ***J***, The average crossing number over the platform-site (***I***) and the latency of the first target-site crossover (probe time; ***J***) during the probe trial. Data are shown as mean ± SD and $n = 10$. Statistically significant $^{*}p < 0.05$, $^{**}p < 0.01$, $^{***}p < 0.001$ versus WT control group; $^{\#\#}p < 0.01$, $^{\#\#\#}p < 0.001$ versus control CRISPR/Cas9–treated group in WT; $^{@@}p < 0.01$ versus WT FPI group in ***A–G***. For graphs ***I*** and ***J***, statistically significant values are given in the graphs. Statistical analysis was performed by two-way ANOVA with Bonferroni's post hoc test.

Even though both receptors LFA-1 and Mac-1 appear to be important in leukocyte adhesion, LFA-1 has more contribution to cell adhesion and transmigration than Mac-1 (Ding et al., 1999; Dunne et al., 2003). Many therapeutic strategies are also focused on LFA-1 by changing its conformation, clustering, or cell signaling (Ding et al., 1999; Dunne et al., 2003); however, defects in LFA-1 cause genetic abnormalities, deficient immune response, and autoimmunity (Springer et al., 1985; Lowin and Straub, 2011).

In the context of these findings, next, we emphasized that brain injury causes BBB damage and increases permeability and leakage to the brain. TBI causes BBB disruption that has important clinical implications (Adams et al., 2018; van Vliet et al., 2020; Kiani, 2022; Sulimai et al., 2023). It can lead to the entry of blood components, immune cells, and potentially harmful substances into the brain, contributing to secondary injury processes like brain edema, inflammation, and long-term neurological deficits (Persidsky et al., 2006; Abdul Muneer et al., 2012; Heinemann et al., 2012; Abdul-Muneer et al., 2015; Ueno et al., 2016; Marchetti and Engelhardt, 2020). However, we mainly focused on the therapeutic side in which ICAM-1 CRISPR/Cas9 treatment can attenuate BBB damage in vitro and in vivo. In this study, we noticed that there are several CD68-positive cells surrounding microvessels showing the infiltration of immune cells across the BBB. This distinctive localization of CD68 surrounding the perivascular region lends inevitable evidence that vascular BBB injury/inflammation paves the path for the infiltration of immune cells across the BBB. This event is functionally validated in the present study by infusing Fluo3-labeled macrophages through the carotid artery, and the infiltration of these cells was analyzed in the brain cortex. Further, we validated that the leakage of NaFl and EB tracers from the blood circulation is possible only if the BBB function is impaired.

Next, we provide evidence of ICAM-1's role in regulating the paxillin and FAK signaling that facilitates leukocyte transmigration in in vitro and in vivo TBI models. Paxillin is a scaffolding protein and a main component of FAs (Burridge et al., 1992; Schaller, 2001). The phosphorylation of paxillin by FAK allows the recruitment of several enzymes and structural molecules, and the association of paxillin with these molecules results in changes in cell movement and migration. In addition, there are reports on the involvement of Src in the phosphorylation of paxillin during cell adhesion and growth factor stimulation. Autophosphorylation of FAK and Tyr phosphorylation of paxillin provides a scaffold for the recruitment of tyrosine kinases FAK and Src. Paxillin phosphorylates at Tyr88 and Tyr118 by Src, as well as at Tyr118 and Tyr31 at the N terminus by FAK (Zaidel-Bar et al., 2007). In this study, we confirmed the involvement of ICAM-1 in the activation of paxillin, FAK, and Src. The phosphorylated form of these three molecules was expressed less in ICAM-1 CRISPR/Cas9 or ICAM-1 siRNA treatment in vitro and ICAM-1 CRISPR/Cas9 treatment and *ICAM-1*$^{-/-}$ animals in vivo.

Rho GTPase signaling plays a crucial role in the regulation of FAs and cell migration (Chen and Gallo, 2012). The FAK/paxillin pathway regulates small Rho GTPases including Rac1, RhoA, and Cdc42, which are critical determinants of leukocyte transmigration (Hodge and Ridley, 2016). Among the members of Rho GTPases, Rac1 and Cdc42 are respectively involved in the formation of lamellipodia and filopodia, whereas RhoA promotes the maturation of adhesion of immune cells (Ridley, 2015). Paxillin coordinates the spatiotemporal activation of Rac1, RhoA, and Cdc42 GTPases by recruiting guanine nucleotide exchange factors (GEFs) and GTPase-activating proteins (GAPs) along with specific effector proteins to FAs, thus regulating cell adhesion and migration (Ridley, 2015). This gives us further room to study the role of ICAM-1 in activating Rho GTPase molecules by recruiting GEFs and GAPs. However, in this study, we analyzed the role of ICAM-1 in the transmigration of leukocytes by phosphorylating paxillin, FAK, Src, and Rac1 and activating RhoA and Cdc42 molecules.

Inflammatory leukocyte adhesion and transmigration cascades are regulated by certain cytokines produced by the inflammatory response. In this study, we demonstrated whether ICAM-1 has any role in the induction of angiogenesis protein VEGF-A, chemoattractant CXCL-8 (IL-8), and two common inflammatory cytokines IL-1β and TNF-α. In our previous study, we found that VEGF-A has a significant role in inducing ICAM-1 (Bhowmick et al., 2021), whereas, in this study, we tried to demonstrate the reverse action, that is, induction of VEGF-A by ICAM-1. Interestingly, we did not notice any effect of ICAM-1 on inducing VEGF-A. CXCL-8 is a chemokine, which induces monocyte extravasation and activates leukocyte integrins. CXCL-8, also known as "neutrophil chemotactic factor," induces chemotaxis in target cells, primarily neutrophils but also other granulocytes, causing them to migrate toward the site of injury or infection (Meliton et al., 2010). Here, we demonstrated that ICAM-1 induces CXCL-8 and other two proinflammatory cytokines IL-1β and TNF-α that have significant roles in the pathophysiology of TBI.

Cognitive impairments, prolonged sensorimotor deficits, and psychological stress behavior are common in TBI patients (Xing et al., 2013; Bhowmick et al., 2018b). The role of ICAM-1 in developing fear and anxiety responses has been previously implicated (Zhang et al., 2017). Recently, we showed that TBI-induced ICAM-1 activation is associated with sensorimotor function impairment and the development of depression and anxiety-like psychological stress behaviors (Bhowmick et al., 2021). In this study, we validated that ICAM-1 activation following TBI impairs sensorimotor function as monitored by the rotarod and grid walk tests and severely exacerbates depression and anxiety-like psychological stress as monitored by the sucrose preference test and the light–dark test. Further, we validated the role of ICAM-1 in the impairment of spatial memory and learning by conducting MWM experiments, and we confirmed that the deletion of ICAM-1 promotes functional recovery from these behavioral impairments following TBI. Together, these findings validate novel evidence for the contribution of ICAM-1 in facilitating brain damage and impairment in functional outcomes following TBI.

In conclusion, the data of this study validates the role of ICAM-1 in the transmigration of leukocytes to the brain by regulating the paxillin/FAK-dependent Rho GTPase pathway following TBI. Moreover, we confirm that the deletion of ICAM-1 promotes functional recovery from sensorimotor functional deficits, psychological stress, and spatial memory and learning impairments. Since the recombinant DNA technology is not feasible for developing a therapeutic strategy against TBI-induced neurological complications, we suggest here that our present study encourages further work on developing a therapeutic strategy targeting ICAM-1 by blocking the biological activity of ICAM-1 using antagonistic peptides.

Data and Materials Availability

The data and materials that support the findings of this study are available from the corresponding author upon reasonable request.

References

Abdul Muneer PM, Alikunju S, Szlachetka AM, Haorah J (2012) The mechanisms of cerebral vascular dysfunction and neuroinflammation by MMP-mediated degradation of VEGFR-2 in alcohol ingestion. Arterioscler Thromb Vasc Biol 32:1167–1177.

Abdul-Muneer PM, Schuetz H, Wang F, Skotak M, Jones J, Gorantla S, Zimmerman MC, Chandra N, Haorah J (2013) Induction of oxidative and nitrosative damage leads to cerebrovascular inflammation in an animal model of mild traumatic brain injury induced by primary blast. Free Radic Biol Med 60:282–291.

Abdul-Muneer PM, Chandra N, Haorah J (2015) Interactions of oxidative stress and neurovascular inflammation in the pathogenesis of traumatic brain injury. Mol Neurobiol 51:966–979.

Abdul-Muneer PM, Bhowmick S, Briski N (2018) Angiotensin II causes neuronal damage in stretch-injured neurons: protective effects of losartan, an angiotensin T1 receptor blocker. Mol Neurobiol 55:5901–5912.

Abdul-Muneer PM, Saikia BB, Bhowmick S (2022) Synergistic effect of mild traumatic brain injury and alcohol aggravates neuroinflammation, amyloidogenesis, tau pathology, neurodegeneration, and blood–brain barrier alterations: impact on psychological stress. Exp Neurol 358:114222.

Adams C, et al. (2018) Neurogliovascular dysfunction in a model of repeated traumatic brain injury. Theranostics 8:4824–4836.

Alikunju S, Abdul Muneer PM, Zhang Y, Szlachetka AM, Haorah J (2011) The inflammatory footprints of alcohol-induced oxidative damage in neurovascular components. Brain Behav Immun 25:S129–136.

Baban B, et al. (2021) AMPK induces regulatory innate lymphoid cells after traumatic brain injury. JCI Insight 6:e126766.

Bankhead P (2014) *Analyzing fluorescence microscopy images with ImageJ*. Northern Ireland: Queen's University Belfast.

Bazzoni G (2011) Pathobiology of junctional adhesion molecules. Antioxid Redox Signal 15:1221–1234.

Bhowmick S, D'Mello V, Abdul-Muneer PM (2018a) Synergistic inhibition of ERK1/2 and JNK, not p38, phosphorylation ameliorates neuronal damages after traumatic brain injury. Mol Neurobiol 56:1124–1136.

Bhowmick S, D'Mello V, Ponery N, Abdul-Muneer PM (2018b) Neurodegeneration and sensorimotor deficits in the mouse model of traumatic brain injury. Brain Sci 8:11.

Bhowmick S, Dmello V, Caruso D, Abdul-Muneer PM (2019a) Traumatic brain injury-induced down regulation of Nrf2 activates inflammatory response and apoptotic cell death. J Mol Med 97:1627–1641.

Bhowmick S, D'Mello V, Caruso D, Wallerstein A, Abdul-Muneer PM (2019b) Impairment of pericyte-endothelium crosstalk leads to blood–brain barrier dysfunction following traumatic brain injury. Exp Neurol 317:260–270.

Bhowmick S, Malat A, Caruso D, Ponery N, D'Mello V, Finn C, Abdul-Muneer PM (2021) Intercellular adhesion molecule-1-induced post-traumatic brain injury neuropathology in the prefrontal cortex and hippocampus leads to sensorimotor function deficits and psychological stress. eNeuro 8:ENEURO.0242-21.2021.

Bui TM, Wiesolek HL, Sumagin R (2020) ICAM-1: a master regulator of cellular responses in inflammation, injury resolution, and tumorigenesis. J Leukoc Biol 108:787–799.

Burridge K, Turner CE, Romer LH (1992) Tyrosine phosphorylation of paxillin and pp125FAK accompanies cell adhesion to extracellular matrix: a role in cytoskeletal assembly. J Cell Biol 119:893–903.

Carpenter AC, Saborido TP, Stanwood GD (2012) Development of hyperactivity and anxiety responses in dopamine transporter-deficient mice. Dev Neurosci 34:250–257.

Chen J, Gallo KA (2012) MLK3 regulates paxillin phosphorylation in chemokine-mediated breast cancer cell migration and invasion to drive metastasis. Cancer Res 72:4130–4140.

Chen GC, Turano B, Ruest PJ, Hagel M, Settleman J, Thomas SM (2005) Regulation of Rho and Rac signaling to the actin cytoskeleton by paxillin during Drosophila development. Mol Cell Biol 25:979–987.

Cuvelier SL, Paul S, Shariat N, Colarusso P, Patel KD (2005) Eosinophil adhesion under flow conditions activates mechanosensitive signaling pathways in human endothelial cells. J Exp Med 202:865–876.

Dietrich JB (2002) The adhesion molecule ICAM-1 and its regulation in relation with the blood–brain barrier. J Neuroimmunol 128:58–68.

Di Fusco D, Dinallo V, Marafini I, Figliuzzi MM, Romano B, Monteleone G (2019) Antisense oligonucleotide: basic concepts and therapeutic application in inflammatory bowel disease. Front Pharmacol 10:305.

Ding ZM, et al. (1999) Relative contribution of LFA-1 and Mac-1 to neutrophil adhesion and migration. J Immunol 163:5029–5038.

Dunne JL, Collins RG, Beaudet AL, Ballantyne CM, Ley K (2003) Mac-1, but not LFA-1, uses intercellular adhesion molecule-1 to mediate slow leukocyte rolling in TNF-alpha-induced inflammation. J Immunol 171:6105–6111.

Etienne-Manneville S, Hall A (2002) Rho GTPases in cell biology. Nature 420:629–635.

Faul F, Erdfelder E, Lang AG, Buchner A (2007) G*Power 3: a flexible statistical power analysis program for the social, behavioral, and biomedical sciences. Behav Res Methods 39:175–191.

Frank PG, Lisanti MP (2008) ICAM-1: role in inflammation and in the regulation of vascular permeability. Am J Physiol Heart Circ Physiol 295:H926–H927.

Heinemann U, Kaufer D, Friedman A (2012) Blood–brain barrier dysfunction, TGFbeta signaling, and astrocyte dysfunction in epilepsy. Glia 60:1251–1257.

Hodge RG, Ridley AJ (2016) Regulating Rho GTPases and their regulators. Nat Rev Mol Cell Biol 17:496–510.

Isaksson J, Lewen A, Hillered L, Olsson Y (1997) Up-regulation of intercellular adhesion molecule 1 in cerebral microvessels after cortical contusion trauma in a rat model. Acta Neuropathol 94:16–20.

Jin W, Wang H, Yan W, Xu L, Wang X, Zhao X, Yang X, Chen G, Ji Y (2008) Disruption of Nrf2 enhances upregulation of nuclear factor-kappaB activity, proinflammatory cytokines, and intercellular adhesion molecule-1 in the brain after traumatic brain injury. Mediators Inflamm 2008:725174.

Kelly KJ, Williams WW Jr, Colvin RB, Meehan SM, Springer TA, Gutierrez-Ramos JC, Bonventre JV (1996) Intercellular adhesion molecule-1-deficient mice are protected against ischemic renal injury. J Clin Invest 97:1056–1063.

Kiani L (2022) Blood–brain barrier dysfunction following TBI. Nat Rev Neurol 18:699.

Kim JY, Grunke SD, Levites Y, Golde TE, Jankowsky JL (2014) Intracerebroventricular viral injection of the neonatal mouse brain for persistent and widespread neuronal transduction. J Vis Exp 15:51863.

Kirsch D, et al. (2023) Vascular injury is associated with repetitive head impacts and tau pathology in chronic traumatic encephalopathy. J Neuropathol Exp Neurol 82:127–139.

Knoblach SM, Faden AI (2002) Administration of either anti-intercellular adhesion molecule-1 or a nonspecific control antibody improves recovery after traumatic brain injury in the rat. J Neurotrauma 19:1039–1050.

Li X, et al. (2016) Mitochondrial reactive oxygen species mediate lysophosphatidylcholine-induced endothelial cell activation. Arterioscler Thromb Vasc Biol 36:1090–1100.

Lowin T, Straub RH (2011) Integrins and their ligands in rheumatoid arthritis. Arthritis Res Ther 13:244.

Luscinskas FW (2012) FAK and PAX-illin get involved in leukocyte diapedesis. Eur J Immunol 42:296–298.

Lutton EM, Razmpour R, Andrews AM, Cannella LA, Son YJ, Shuvaev VV, Muzykantov VR, Ramirez SH (2017) Acute administration of catalase targeted to ICAM-1 attenuates neuropathology in experimental traumatic brain injury. Sci Rep 7:3846.

Marchetti L, Engelhardt B (2020) Immune cell trafficking across the blood–brain barrier in the absence and presence of neuroinflammation. Vasc Biol 2:H1–H18.

Meliton AY, Munoz NM, Meliton LN, Binder DC, Osan CM, Zhu X, Dudek SM, Leff AR (2010) Cytosolic group IVa phospholipase A2 mediates IL-8/CXCL8-induced transmigration of human polymorphonuclear leukocytes in vitro. J Inflamm 7:14.

Mulherkar S, Tolias KF (2020) RhoA-ROCK signaling as a therapeutic target in traumatic brain injury. Cells 9:245.

Muradashvili N, Benton RL, Saatman KE, Tyagi SC, Lominadze D (2015) Ablation of matrix metalloproteinase-9 gene decreases cerebrovascular permeability and fibrinogen deposition post traumatic brain injury in mice. Metab Brain Dis 30:411–426.

Ohtake Y, Park D, Abdul-Muneer PM, Li H, Xu B, Sharma K, Smith GM, Selzer ME, Li S (2014) The effect of systemic PTEN antagonist peptides on axon growth and functional recovery after spinal cord injury. Biomaterials 35:4610–4626.

Parsons SA, Sharma R, Roccamatisi DL, Zhang H, Petri B, Kubes P, Colarusso P, Patel KD (2012) Endothelial paxillin and focal adhesion kinase (FAK) play a critical role in neutrophil transmigration. Eur J Immunol 42:436–446.

Patel RK, Prasad N, Kuwar R, Haldar D, Abdul-Muneer PM (2017) Transforming growth factor-beta 1 signaling regulates neuroinflammation and apoptosis in mild traumatic brain injury. Brain Behav Immun 35:4610–4626.

Persidsky Y, Ramirez SH, Haorah J, Kanmogne GD (2006) Blood–brain barrier: structural components and function under physiologic and pathologic conditions. J Neuroimmune Pharmacol 1:223–236.

Powell TR, Fernandes C, Schalkwyk LC (2012) Depression-related behavioral tests. Curr Protoc Mouse Biol 2:119–127.

Ridley AJ (2015) Rho GTPase signalling in cell migration. Curr Opin Cell Biol 36:103–112.

Romanova LY, Mushinski JF (2011) Central role of paxillin phosphorylation in regulation of LFA-1 integrins activity and lymphocyte migration. Cell Adh Migr 5:457–462.

Schaller MD (2001) Paxillin: a focal adhesion-associated adaptor protein. Oncogene 20:6459–6472.

Schmidt SI, Blaabjerg M, Freude K, Meyer M (2022) Rhoa signaling in neurodegenerative diseases. Cells 11:1520.

Schmitz B, et al. (2013) Increased monocyte adhesion by endothelial xpression of VCAM-1 missense variation in vitro. Atherosclerosis 230:185–190.

Schwarzmaier SM, Zimmermann R, McGarry NB, Trabold R, Kim SW, Plesnila N (2013) In vivo temporal and spatial profile of leukocyte adhesion and migration after experimental traumatic brain injury in mice. J Neuroinflammation 10:32.

Sha X, Meng S, Li X, Xi H, Maddaloni M, Pascual DW, Shan H, Jiang X, Wang H, Yang XF (2015) Interleukin-35 inhibits endothelial cell activation by suppressing MAPK-AP-1 pathway. J Biol Chem 290:19307–19318.

Springer TA, Rothlein R, Anderson DC, Burakoff SJ, Krensky AM (1985) The function of LFA-1 in cell-mediated killing and adhesion: studies on heritable LFA-1, Mac-1 deficiency and on lymphoid cell self-aggregation. Adv Exp Med Biol 184:311–322.

Sulimai N, Brown J, Lominadze D (2023) Vascular effects on cerebrovascular permeability and neurodegeneration. Biomolecules 13.

Ueno M, Chiba Y, Matsumoto K, Murakami R, Fujihara R, Kawauchi M, Miyanaka H, Nakagawa T (2016) Blood–brain barrier damage in vascular dementia. Neuropathology 36:115–124.

van Vliet EA, Ndode-Ekane XE, Lehto LJ, Gorter JA, Andrade P, Aronica E, Grohn O, Pitkanen A (2020) Long-lasting blood–brain barrier dysfunction and neuroinflammation after traumatic brain injury. Neurobiol Dis 145:105080.

Vorhees CV, Williams MT (2006) Morris water maze: procedures for assessing spatial and related forms of learning and memory. Nat Protoc 1:848–858.

Whalen MJ, Carlos TM, Dixon CE, Schiding JK, Clark RS, Baum E, Yan HQ, Marion DW, Kochanek PM (1999) Effect of traumatic brain injury in mice deficient in intercellular adhesion molecule-1: assessment of histopathologic and functional outcome. J Neurotrauma 16:299–309.

Witcher KG, et al. (2021) Traumatic brain injury causes chronic cortical inflammation and neuronal dysfunction mediated by microglia. J Neurosci 41:1597–1616.

Xing G, Barry ES, Benford B, Grunberg NE, Li H, Watson WD, Sharma P (2013) Impact of repeated stress on traumatic brain injury-induced mitochondrial electron transport chain expression and behavioral responses in rats. Front Neurol 4:196.

Xu S, et al. (2019) An HK2 antisense oligonucleotide induces synthetic lethality in HK1(-)HK2(+) multiple myeloma. Cancer Res 79:2748–2760.

Xu K, et al. (2022) Monocyte adhesion assays for detecting endothelial cell activation in vascular inflammation and atherosclerosis. Methods Mol Biol 2419:169–182.

Zaidel-Bar R, Milo R, Kam Z, Geiger B (2007) A paxillin tyrosine phosphorylation switch regulates the assembly and form of cell-matrix adhesions. J Cell Sci 120:137–148.

Zhang Q, Zhang J, Yan Y, Zhang P, Zhang W, Xia R (2017) Proinflammatory cytokines correlate with early exercise attenuating anxiety-like behavior after cerebral ischemia. Brain Behav 7:e00854.

Zhao Z, Nelson AR, Betsholtz C, Zlokovic BV (2015) Establishment and dysfunction of the blood–brain barrier. Cell 163:1064–1078.